GAS GUN STUDIES OF ARMATURE-RAIL INTERFACE WEAR EFFECTS

A Thesis
Presented to
The Academic Faculty

by

Tyler Andrew Jackson

In Partial Fulfillment
of the Requirements for the Degree
Master of Science in Mechanical Engineering in the
School of Mechanical Engineering

Georgia Institute of Technology
December 2010

GAS GUN STUDIES OF ARMATURE-RAIL INTERFACE WEAR EFFECTS

Approved by:

Dr. Naresh Thadhani, Advisor
School of Mechanical Engineering
Georgia Institute of Technology

Dr. Rick Cowan
Manufacturing Research Center
Georgia Institute of Technology

Dr. Steven Danyluk
School of Mechanical Engineering
Georgia Institute of Technology

Dr. David Rosen
School of Mechanical Engineering
Georgia Institute of Technology

Date Approved: 10 November 2010

This work is dedicated to those who encourage others to learn and search for new ideas.

Without teachers and mentors to help develop the minds of the next generation we would

surely be at a loss.

ACKNOWLEDGEMENTS

TABLE OF CONTENTS

LIST OF TABLES

LIST OF FIGURES

SUMMARY

The objective of this work has been to investigate the applicability of the gas gun to study the characteristics of interface wear during acceleration of an aluminum rod through a hollow copper wedge. The study of wear characteristics is important in applications such as armature-rail interaction during railgun operation. The approach involved developing coefficients of constitutive strength models for aluminum 6061 as well as oxygen-free high-thermal conductivity copper, and using those to design the die geometry for performing interface wear studies using the gas gun. Taylor rod-on-anvil impact experiments were performed to validate the accuracy of constitutive strength models by correlating experimentally obtained deformed states of impacted samples with those predicted using ANSYS AUTODYN hydrocode. An optical comparator was used to discretize the cross sectional deformation profile of each impacted rod-shaped sample. Parameters of the Johnson-Cook strength model were adjusted for each material to match deformation profiles obtained from simulations with profiles obtained from impact experiments. The fitted Johnson-Cook model parameters for each material were able to give overall deformed length and diameter values within 2% of the experimentally observed data. Simulations were then used with the validated strength model parameters to design the geometry involving acceleration of cylindrical rods of aluminum through a concentric cylindrical angular extrusion die made of copper. Experiments were conducted using this geometry and employing both the 7.62mm and 80mm diameter gas guns. Microstructural analysis was conducted on Al-Cu interfaces of the recovered samples from both designs. Hardness measurements were also performed along the interface to evaluate the properties of the interface layer and determine the structure formation due to solid-state wear or melt formation. The stress and strain conditions resulting in the observed microstructural effects were correlated with predictions from numerical simulations performed using the validated material models. The overall results illustrate that the stress-strain conditions produced during acceleration of aluminum

through the hollow concentric 5° copper angular die, result in interface deformation and wear characteristics that are influenced by velocity. At velocities (less than about 800m/s), interface wear leads to formation of a layer dominated by solid-state alloying of Cu and Al, while higher velocities produce an interface layer consisting of only melted and re-solidified aluminum. The variation of the structural characteristics of the interface layer as a function of velocity are similar to those observed during armature-rail interactions in railgun operation, although at a much higher velocity regime, and with superimposed electric and magnetic field effects. Nevertheless, the results of the present work illustrate that the setup employed using the gas gun can enable studies of the characteristics of interface wear as a function of velocity, die angle, and material types, in order to generate a fundamental understanding of dynamic friction and sliding between dissimilar materials subjected to high-strain-rate loading applications.

CHAPTER I

INTRODUCTION

Studies of characteristics of interface wear during acceleration of one metal against another metal are of importance in a number of applications involving dynamic high-strain-rate loading. One such application is associated with armature-rail interaction during operation of a railgun or electromagnetic launcher. Several large facilities have been constructed including the Green Farm facilities in California, operated by the Defense Nuclear Agency, and another at IAT Dahlgren to investigate whether railguns could be used to accelerate large projectiles to velocities greater than those achieved with conventional propellant-driven guns. Both have been able to accelerate 1-2kg packages to 2.5-4km/s. Most of the fundamental research in the U.S. has been focused on solid armatures and the physics of current carrying metal contacts sliding at hypervelocities [4].

An important aspect of railgun operation that has not been fully investigated is the armature-rail interface wear effects. During operation the armature-rail interface experiences both Joule heating from the current and frictional heating from sliding of the armature against the rail material. Research is being done to effectively model the conditions at the interface and better study the effects of melt lubrication and deposit build up on rail life. Other applications where studies of interface wear and sliding are important include projectile acceleration in gun barrels, and in fact any scenario of high-velocity impact of an object against a stationary or moving target. Effects of interface wear are also important during high-rate compaction of particulate media involving similar or dissimilar constituents.

Most studies of interface wear are often investigated during operation of actual devices, which limits observation of the progression and variation of processes and therefore a clear understanding of the mechanisms and parameters influencing the observed effects. Hence, there is a need to develop test techniques that can be employed to emulate and provide a controlled system for studies of interface wear over a range of loading conditions, and for

easily changeable materials systems.

The objective of the research performed in this work has been to investigate the applicability of the gas guns to study the characteristics of interface wear during acceleration of an aluminum rod through a hollow copper wedge. The approach involved the use of Taylor rod-on-anvil impact tests to first obtain the coefficients and validate the Johnson-Cook constitutive strength model by correlating the simulated deformed states of impacted aluminum and copper rods with those obtained from experiments. These validated strength models were then used to design a hollow concentric angular die setup through which an aluminum rod was accelerated. The interface wear resulting from the longitudinal force was established by the die angle and velocity. Microstructural analysis and microhardness measurements were performed to evaluate the structural characteristics of the Al-Cu interface layer, and correlate those with the stress-strain conditions generated as a function of velocity.

This thesis will begin with a background chapter providing overview of an application of a system influenced by interface wear characteristics, namely, due to armature-rail interaction in a railgun. The fundamentals of high-strain-rate deformation, namely examples of a physically based and empirical constitutive strength models will also be presented in the background Chapter 2. Experimental procedures for the Taylor test and concentric die design are outlined in Chapter 3. Chapter 4 describes the numerical simulations performed using ANSYS AUTODYN for the validation of the material models and subsequent design of the die. Results of the experiments and their comparison to simulations for model verification and description of stress-strain conditions, along with key features of interface effects studied using a variety of microscopy techniques, will be presented and discussed in Chapter 5. Concluding remarks and recommendations for future work are described in Chapter 6.

CHAPTER II

BACKGROUND

Interface wear during sliding of one metal against another at high velocities is dominated by conditions of high-strain-rate deformation. Under these conditions, the strength of the materials is influenced by competing effects of strain, strain rate hardening, and thermal softening. High rate severe plastic deformation can also result in grain size refinement and even melting. An application where such effects are most dominant is during the armature-rail interaction associated with the operation of a railgun. In this chapter a brief review of the railgun, along with the characteristics of the interface layer, will be described. This will be followed by a brief description of constitutive strength models relevant to high-strain-rate deformation, including the physically based Steinberg-Guinan model and the Johnson-Cook empirical model.

2.1 Railgun Overview

Electromagnetic launchers (railguns) are able to accelerate projectiles in excess of 2km/s. With higher velocities and shorter flight times the effective range is increased and there are different kinetic interactions with target materials [4]. An electromagnetic railgun works by passing electrical current from a pulsed power supply along conducting rails. The rails are connected by a metal armature which has the launch package integrated to its form, Figure 1. Current passing through the rails creates a magnetic field which interacts with the current in the armature, which generates a Lorentz force that accelerates the launch package along the length of the rails [1].

Railgun operation relies on the use of the magnetic field generated by a moving charge or current. As the current $\vec{I}$ passes along a wire, magnetic field $\vec{B}$ forms around the current and obeys the right-hand rule as shown in Figure 2.
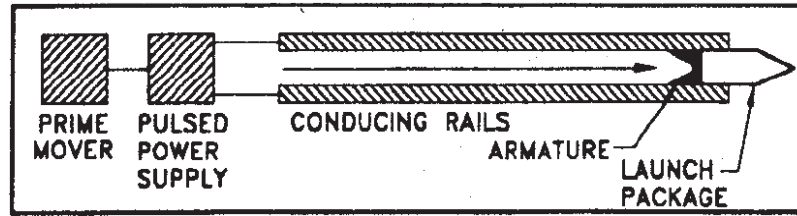
Figure 1: Schematic of the fundamentals of railgun operation [1]
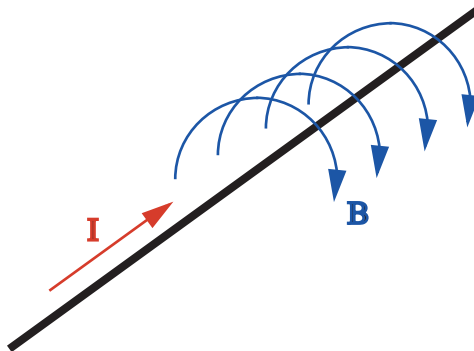
Figure 2: Current $\vec{I}$ traveling along a wire generates magnetic field $\vec{B}$ according to the right-hand rule principle [2].

When a charged particle moves through an electrical field $\vec{E}$ and a magnetic field $\vec{B}$ it experiences both electrical and magnetic forces. The combined force is known as the Lorentz force, $\vec{F}$, and is shown below.

$$\sum \vec{F} = q\vec{E} + q\vec{v} \times \vec{B} \tag{1}$$

where $\vec{v}$ is the velocity vector of the charge q. In a railgun current travels along the two copper rails in opposite directions. The resulting magnetic field between the rails generates a Lorentz force acting on the current moving through the aluminum armature and causes the armature and launch package to accelerate. Research is being done to study the ability to launch projectiles at velocities greater than conventional propellant guns that are limited by the sound speed in the propellant medium. For many U.S. military missions, velocities of interest are 2-3km/s. It has been found that in this range, solid armatures are more energy efficient than plasma armatures using liquid metal [5].

2.2 Armature-Rail Interface

Much attention has been given to the design of high-performance armatures. Research during the 1970's at the Australian National University [6], [7], has shown difficulties in developing these armatures and the importance of armature-rail interface phenomena. In the U.S., fundamental research is centered on solid armatures, typically of aluminum. Solid armatures are described as a forced movable conductor contained between two stationary conducting rails, as shown in Figure 1. Its purpose is to transmit acceleration forces to the launch package [5]. During railgun operation, Joule heating of the armature occurs as current passes through the conducting metal components. Frictional heating also takes place as the armature travels along the length of the rails. Another important phenomena is the velocity skin effect [8]. At low speeds the distribution of current throughout the armature is uniform. However, at high velocities the distribution is shifted, with up to 80% concentrated in the rear 2% of the armature, as illustrated in Figure 3. This constriction of the current and increased resistance in the interface layer acts as both an energy loss and heat source.
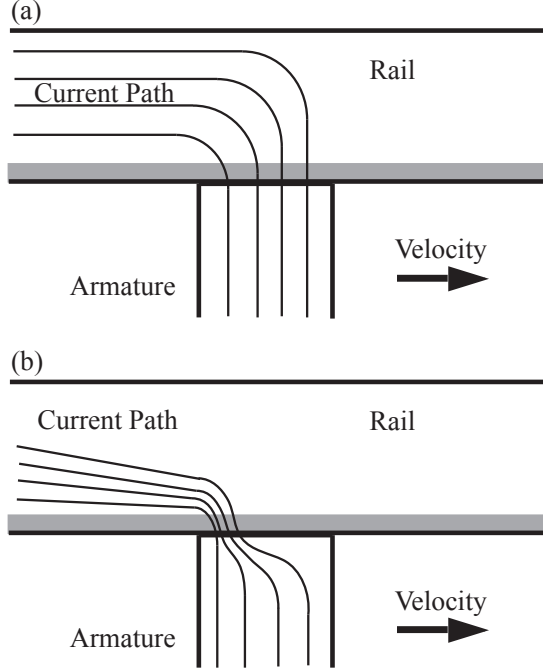
Figure 3: Velocity skin effect in the rail, interface layer, and armature cause current constriction and resistance changes in these regions. (a) Low velocity (b) High velocity

Armature-rail contact in a railgun often experiences a change from low-voltage to high-voltage contact, called "transition". To give a good indication of the armature-rail contact voltage the muzzle voltage is measured during a railgun experiment. Figure 4 shows a typical muzzle voltage reading during an experiment and the increase from 30V to over 400V is indicative of transition [9]. Temperatures in the interface often exceed the melt temperature for the aluminum armature and liquid metal is formed along the interface. As the armature melts it can lose contact with the rail. Arcs form between the rail and armature. "Transition" in a railgun signals this plasma contact at the armature-rail interface, instead of solid or liquid metal-to-metal contact. Plasma contact also results in a loss of efficiency for the railgun.
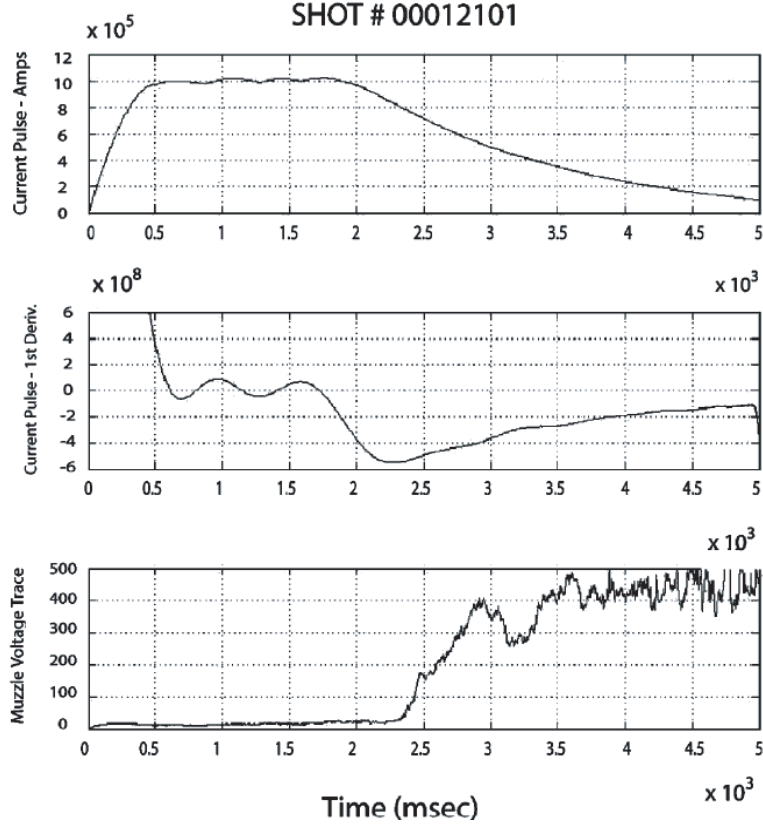
Figure 4: Muzzle voltage trace during railgun operation increases abruptly during the down-slope of the current, indicating armature transition.

2.2.1 Liquid Metal Effects

The melted layer generated at the armature-rail interface has many important effects on the efficiency of the rail-gun performance. Firstly, it provides melt lubrication to the armature. Experimental studies have found very low frictional coefficients for solid aluminum armatures on copper rails [10]. To calculate the frictional force in these studies, researchers first determine the Lorentz accelerating force generated from the known power inputs. Launch velocity can be experimentally observed and the Newtonian (F=ma) accelerating force required for the velocity can be calculated. The frictional force is then estimated as the difference in the Lorentz and Newtonian forces. Many calculations of the frictional force have given values very close to zero. This has been interpreted to mean a transient liquid layer formed at the armature-rail interface.

7

In the experiments in which zero friction is calculated between the contact of the aluminum armature with the copper rails there have been observations of quenched metallic deposits on the recovered rail surfaces, shown in Figure 5 [11], [12]. This indicates that rather than erosion of the rails, a thin layer of aluminum ($< 25\mu m$) is being loosely deposited. Deposit accumulation and its effects on rail life are frequently expressed operational concerns. Another more fundamental concern is the degree to which this deposit process can be controlled during actual operation [3].
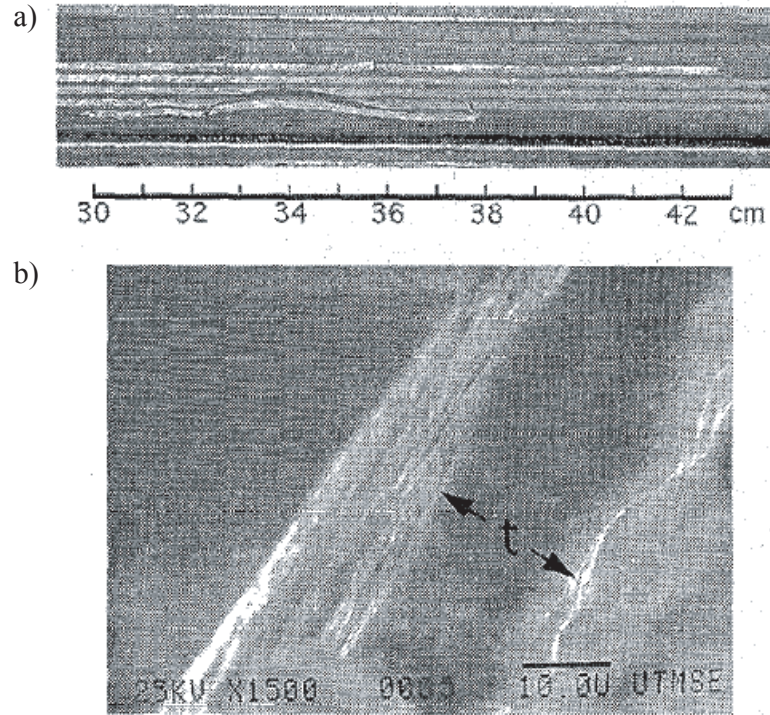
Figure 5: a) The appearance of quenched metal deposit on the rail surface is observed. b) SEM image of a detached film. The film thickness is less than 25μm [3]

2.2.2 Simulations and Experimental Studies

Different models and theories have been developed to describe the electrical contact of the sliding armature. The first theories regarding sliding electric contacts were developed by Holm in the 1960's [13]. Other research by Rabinowics [14] and Kuhlman-Wilsdorf [15] in the 1960's and 1980's has focused on calculating interface temperatures. During operation, these temperatures are often high enough to cause armature melting. It has been difficult to

give a detailed model of the interface due to the transient nature of the conditions. Recent attempts at describing a transient melt wave have been undertaken by Parks [16] and by Barber and Dreizin [17] in the 1990's. Parks [16] presented a current melt-wave model to be used with transitioning solid armatures. Barber and Dreizin [17] developed a model for the contact transitioning with a "realistic" armature-rail interface. Their work combined the velocity skin effect driven melt-wave models that assume a perfect, resistance-free contact with contact resistance models that neglect velocity effects. This combination gives a more realistic picture of this interface phenomena. However, even this model fails to explain all of the results observed by railgun researchers such as a parabolic melt region in a recovered aluminum armature described by Heyse and Jamison [18]

Different experiments and simulations have been developed to study the effects of the armature-rail interface melting. One such approach presented by Angeli [19] focused on the decrease in acceleration and deterioration of the rail caused by the velocity skin effect. He proposed an alternative configuration implementing a muzzle fed railgun with two sets of rails and current moving along the length of the rail in front of the armature in opposite direction to conventional railguns. Hildenbrand [20] studied models and experiments concerned with wear of the armature and how that affects the loss of armature to rail contact area. In Ferrentino's work [21] he described the use of these models and incorporation of proper heating analysis to design integrated metal armatures with copper fibers that would not separate from the rails and arc or cause rail decay. Some efforts have used a modified railgun with one side made of clear material to allow for high speed photography and instrumented armatures and rails to study the effects of initial loading and armature performance [22]. With the amount of interest in understanding the armature-rail interface wear and friction effects, this work was developed to include both simulations and experimentation.

2.3   Dynamic Deformation and Strength Models

It has generally been seen that materials experience a change in their mechanical response under high-strain-rate loading. Constitutive equations are used to describe the plastic deformation in materials during high-strain-rate conditions. These equations relate the

stress in the material with strain, strain rate, and sometimes temperature, illustrated below,

$$\sigma = f(\epsilon, \dot{\epsilon}, T) \tag{2}$$

where ϵ is the strain, $\dot{\epsilon}$ is the strain rate, and T is the temperature. Observations show that at higher strain rates the yield stress of the material increases. Temperature also affects the yield stress response to increased strain rate. At lower temperatures the increase of yield stress with strain rate is more marked [23]. Constitutive equations seek to capture these effects. Various constitutive models including those that are physically based rate-dependent (Zerrilli-Armstrong) and rate-independent (Steinberg-Guinan), as well as those that empirical in nature (Johnson-Cook) are available.

The Zerilli-Armstrong [24] model is a physically based microstructural model that focuses on thermally activated dislocation motion, illustrated below

$$\sigma = C_1(-C_3 T + C_4 T \ln(\dot{\epsilon})) \tag{3}$$

where the C_i constants relate the temperature, T, and strain rate, $\dot{\epsilon}$, to the yield stress, σ. This model is more applicable to bcc metals and thus not considered for copper and aluminum which are fcc metals.

The constitutive equation developed by Steinberg-Guinan [25] which gives the yield stress, σ, was available in the AUTODYN library as shown below,

$$\sigma = \sigma_0 \left\{ 1 + \frac{\sigma'_P}{\sigma_0} \frac{p}{\eta^{1/3}} + \frac{\tau'_T}{\tau_0}(T - 300)(1 + \beta\epsilon)^n \right\} \tag{4}$$

where σ'_P is the derivative of stress with respect to pressure, σ_0 is the stress at the reference temperature and pressure, τ'_T is the derivative of shear stress with respect to temperature, τ_0 is the shear stress at the reference conditions, β is the hardening constant, n is the hardening exponent, and η is the compression v_0/v.

The Johnson-Cook model [26] is an empirical model that includes isotropic strain hardening, strain rate sensitivity, and thermal softening and is expressed as,

$$\sigma = (\sigma_y + B\epsilon^n)(1 + C \ln \dot{\epsilon}^*)(1 - T^{*m}) \tag{5}$$

where $\dot{\epsilon}^*$ and T^* are the normalized strain-rate and temperature, respectively, with material constants σ_y, B, C, n and m. Constants B and n represent the effect of strain hardening,

and the constants C and m represent the effects of strain-rate and temperature, respectively. The parameters for the Johnson-Cook model are determined from experimental observations.

The Taylor rod-on-anvil impact test provides a well suited method for determining the parameters of different constitutive equations. It involves impacting a cylinder of specimen material against a rigid anvil plate to record the deformation response. Experiments are conducted at high strain rates, on the order of $10^4 - 10^6 s^{-1}$ [27]. Recovered samples are able to give the cross section deformation profiles that include the plastic response, captured in deformation localized at the specimen-target interface, and deformation propagation along the specimen from work hardening. Different constitutive models are used in numerical simulations to predict the deformation response for comparison with the experimental results to obtain the strength model parameters.

CHAPTER III

EXPERIMENTAL PROCEDURE

To study characteristics of interface wear during acceleration of one metal against another, a variety of experimental steps were undertaken. First, Taylor rod-on-anvil impact tests were conducted to determine the dynamic high-strain-rate deformation response of aluminum 6061 and OFHC copper using the 7.62mm gas gun. The deformed states of impacted samples were compared with those obtained from numerical simulation predictions to validate constitutive strength model parameters. Experiments were then designed using the validated simulation models that featured rod-shaped aluminum projectiles accelerated through a concentric copper die geometry to study interface wear effects such as those associated with armature-rail interactions. Both the 7.62 and 80mm gas guns were used with similar designs to accelerate the aluminum rod through the copper die at various velocities and study the effects of interface wear.

3.1 Taylor Rod-on-Anvil Impact Test

Taylor rod-on-anvil impact tests were first performed on the aluminum 6061 and copper to generate coefficients and validate constitutive models. For the Taylor rod-on-anvil impact tests, a 7.62mm diameter 1.8m long gas gun at the Georgia Institute of Technology's High-Strain-Rate Laboratory was used, to accelerate a 7.62mm diameter 30mm long cylinder of aluminum and copper. Each sample cylinder is lapped parallel to within $0.01°$ using a 15μm diamond suspension, to ensure planar parallel impact. Since the recovered samples are analyzed for their deformation profiles, the velocity must be such that the projectiles do not fracture or petal upon impact. Input velocities for aluminum and copper cylinders were chosen as 250 and 155m/s, respectively. Compressed helium gas was used to accelerate the projectile and impact a quasi-rigid steel anvil made from high strength and high rigidity Eglin steel contained in the experiment chamber, illustrated in Figure 7. The sides and front of the chamber were fitted with padded material to allow safe sample recovery and

12

minimize any secondary damage to the rod-shaped sample after impact. The chamber is also held under a vacuum of 30-70mTorr. As part of the setup, a laser beam interruption system was placed at the muzzle end of the barrel at known distance from the anvil. The output of the laser detectors goes through a conditioning transistor circuit to convert the signal into a rising TTL pulse. This pulse is fed to an up-down counter (UDC). The distance between the two lasers (D1) and distance from the second laser to the anvil (D2) are entered into the UDC. When the first beam is triggered the UDC begins counting up at a given rate. Once the second beam is triggered the UDC begins counting down at a modified rate of D1/D2. The counter then calculates the velocity of the projectile and also determines the time of impact at the anvil, which is used to trigger the high speed IMACON 200 camera for capturing the images of the impact at various specified times. The images are used to ensure perpendicular impact of the sample with the anvil face. Image analysis also provides measurements of the profile of the projectile during the transient deformation process. Figure 6 shows an example of images of a Taylor impact sample and the transient deformation profile.
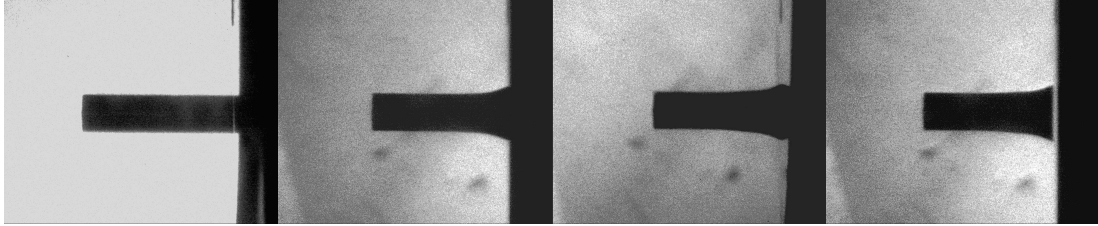
Figure 6: High speed camera images of Taylor rod-on-anvil impact test showing perpendicular impact and the transient deformation profile.

After impact the projectile is recovered from the experiment chamber. An optical comparator is used to measure the x- and y-coordinates of points along the profile of the recovered specimen. In the comparator a magnified silhouette of the sample is projected onto the screen and the dimensions are measured with an accuracy of 2.54μm. These points are then plotted in Excel to produce a 2D cross sectional profile of the final deformed state geometry. The transient deformation state images captured by the camera were also profiled, to allow subsequent comparison of predicted transient and final state profiles obtained in numerical

simulations (described in Chapter 4).
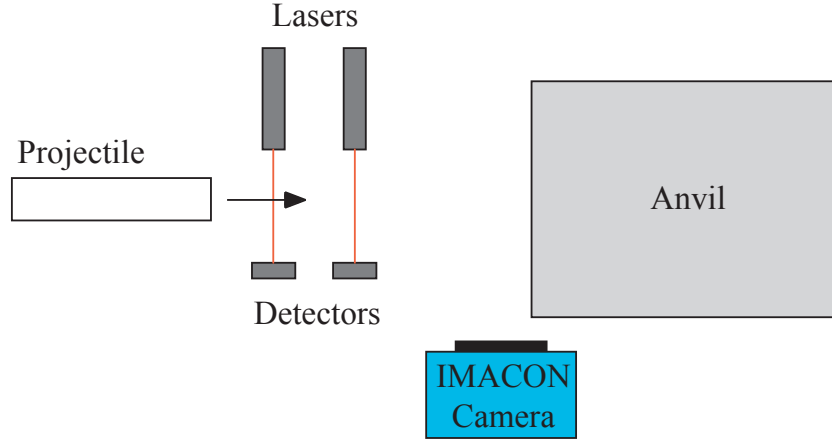
Figure 7: Schematic of Taylor rod-on-anvil impact test setup featuring projectile, laser beam interrupt velocity measurement system, high speed camera, and anvil.

3.2   Gas Gun Concentric Die Design and Experiments

Based on validation of constitutive models obtained from Taylor rod-on-anvil impact tests, hollow concentric copper angular dies were designed for experiments conducted to investigate sliding contact and friction between an aluminum rod and copper die over a velocity range of 250-1000m/s. The 7.62mm diameter gas gun was used to perform three experiments at 250, 500, and 700m/s, and the 80mm gas gun was used for experiments at 880 and 915m/s. It should be noted that the die designs with various taper angles and velocities of aluminum rod accelerated through hollow copper die were explored through AUTODYN simulations. However, the gas gun experiments were performed using the die setup with a constant 5° taper angle and velocity range possible with the 7.62 and 80mm gas guns that would provide the widest variation of results in terms of interface wear characteristics and be consistent with predictions from numerical simulation (described in Chapter 4). Care was taken preparing the samples and in performing experiments, to avoid repetition because of associated costs. Furthermore, while the 7.62mm gun was used for experiments at velocities up to 700m/s and the 80mm gas gun was used for experiments above 800m/s, duplicate experiments with the two guns at the same velocity were not performed. While

it may be good to determine the effect of gas gun loading system per se, no obvious differences in interface wear characteristics are expected with the use of a common die design, as inertial effects dominate the overall material response under these high-rate loading conditions. The hollow cylindrical OFHC copper die with the 5° taper angle, and dimensions of 60mm length, 30mm outer diameter, and 13.7mm and 3.18mm entry and exit diameter was used with the 7.62mm gas gun. A larger steel cylinder housing was used to position the die within it, and restrict its deformation in the radial direction. The die and housing were then mounted to the front of a steel catch tank filled with rags for safe sample recovery. Figure 8 shows the different components, and the die mounted on the catch tank. Test samples of 7.62mm diameter, 30mm length aluminum cylinders were accelerated using the 7.62mm helium gas gun and the laser beam interruption method was used for velocity measurement. The die and catch tank were aligned in the experiment chamber to insure proper acceleration of the projectile into and through the hollow die. Figure 9, shows a cross section of the experimental setup, employed with the 7.62mm gas gun.
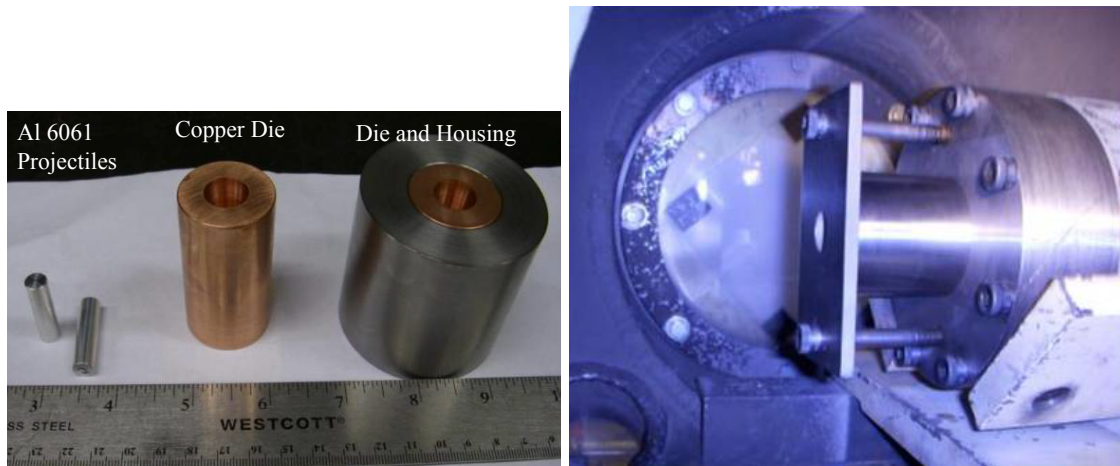
Figure 8: Components of 7.62mm gas gun concentric die experiment and components mounted to catch tank in experiment chamber.

After the experiment the copper die, with embedded aluminum, was pressed out of the steel housing. Some pieces of extruded aluminum fractured, but were captured in the soft recovery catch tank. The copper die was sectioned using a precision cutoff saw to reveal the embedded aluminum sample. The cross-sectioned sample was then polished for imaging and other post processing. Figure 10 illustrates images of the cross section of the copper die and

15
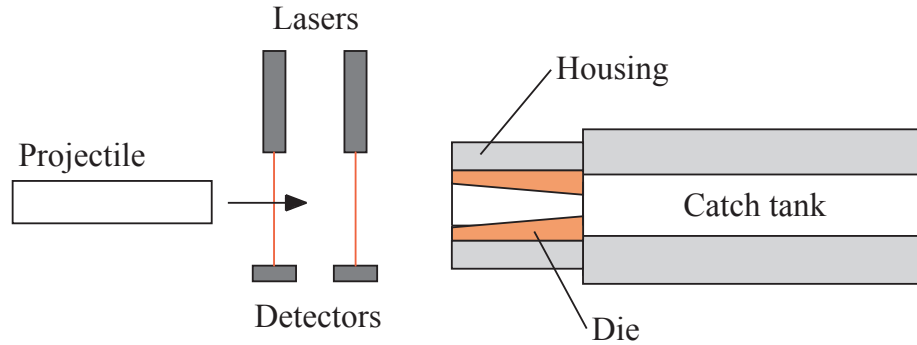
Figure 9: Schematic of 7.62mm gas gun concentric die experiment setup featuring projectile, laser beam interrupt velocity measurement system, and die with housing mounted to catch tank.
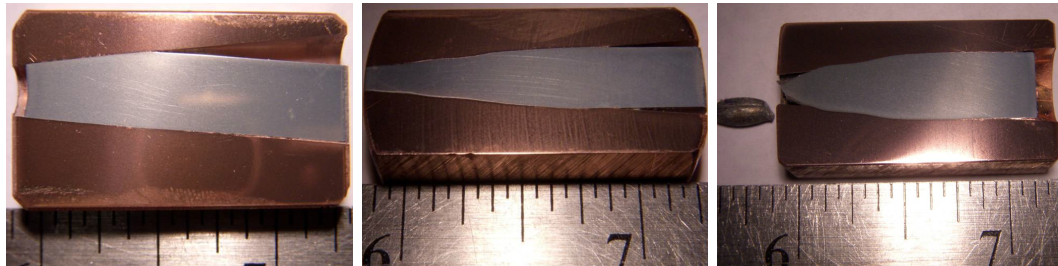
Figure 10: Polished cross sections of 7.62mm gas gun concentric die recovered from 250, 500, and 700m/s experiments.

embedded aluminum rod from the three experiments performed at the various velocities.

The 80mm diameter 8m long gas gun system was used for experiments performed at velocities of 880 and 915m/s. In this case the 7.62mm diameter aluminum rod was mounted to the front face of a 80mm diameter high density polyethylene sabot. The sabot and projectile were accelerated through the length of the barrel with the high pressure helium released upon bursting a double rupture diaphragm. At the muzzle end of the barrel the die setup was mounted to the muzzle face on three 55mm PMMA standoffs. The die setup, shown in Figure 11, was of similar overall geometry as for the 7.62mm gun. It consisted of a 1/4" steel alignment plate with a bolt pattern to match the standoffs and a recessed pocket with through hole for mounting the die and housing. A PMMA plate was used to secure the die and housing to the alignment plate. This securing plate also had a centered hole for a photon doppler velocimetry (PDV) probe, used to measure the incoming projectile velocity. A secondary velocity measurement system incorporated an array of three self shorting crush

pins attached to the muzzle face. A voltage source supplied power to the pins and as the sabot contacted each, a series of up-down counters recorded the time between pin contacts. With the distance between the pins known, the velocity could be recorded.
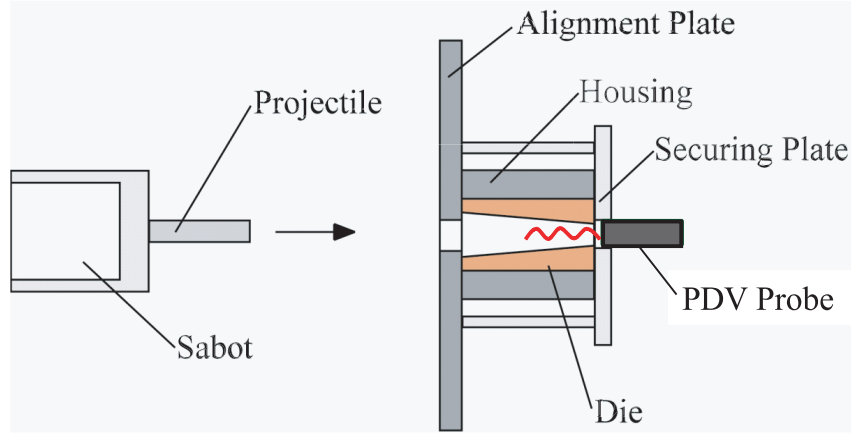
Figure 11: Schematic of 80mm gas gun concentric die experiment setup featuring projectile on sabot, alignment plate for mounting die and housing, securing plate, and PDV probe.

The hollow concentric die design for the 80mm gas gun setup had overall length and diameter dimensions of 40mm and 20mm, respectively. Two designs were developed for the interior surface. One featured a constant 5° tapered hole the entire length of the die, with entry and exit diameters of 10mm and 3.3mm respectively. The other design featured a hybrid of a 5° tapered hole (with entry diameter of 10mm) for the first 30mm of die length and, for the remaining 10mm, a constant cross sectional hole of diameter 5.12mm. Both designs are shown in Figure 12. The constant 5° hollow taper die was used for the experiment performed at 880m/s, and the hybrid die was used for the experiment at 915m/s. The copper die and surrounding steel housing were recovered from the catch tank following with experiments in which the aluminum rad was fully extruded through the die. The die was then sectioned with a precision cutoff saw to reveal the inner die surface. The face was then polished to allow for microstructural analysis. Figure 13 shows examples of the polished sections of the die.
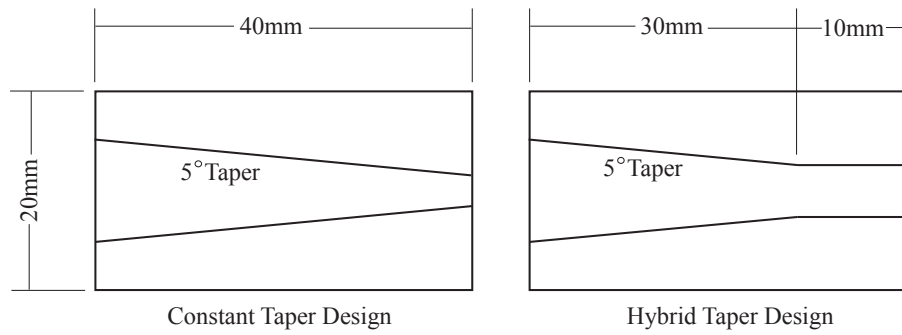
Figure 12: Die designs feature both a constant taper cross section and a hybrid design with constant diameter portion of diameter 5.12mm.
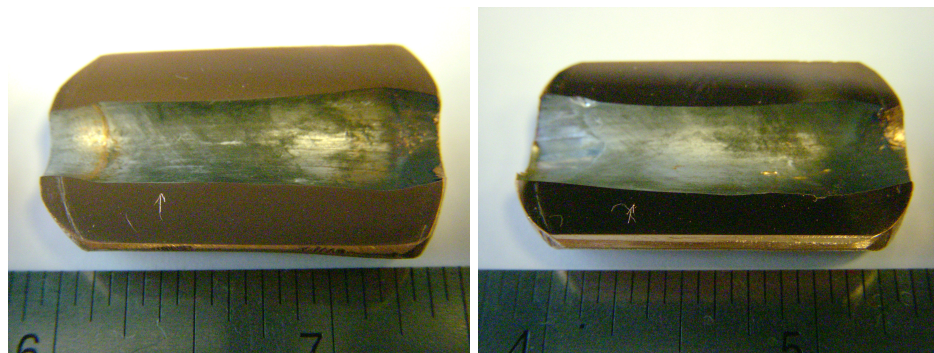
Figure 13: Polished cross sections of 80mm gas gun concentric die at 880 and 915m/s.

CHAPTER IV

NUMERICAL SIMULATIONS

Numerical simulations for this work were performed using ANSYS AUTODYN which is a commercial finite-element software package specializing in dynamic simulations. Numerical simulations with AUTODYN-3D were first used to obtain coefficients for the Johnson-Cook constitutive strength model. This was done by correlating simulated deformation states of impacted Taylor rod samples of Al 6061 and OFHC copper and correlating those to states recovered from actual experiments. Next, the validated models were used with AUTODYN to design the concentric hollow taper copper die for use with the 7.62 and 80mm gas guns.

4.1   Taylor Rod-on-Anvil Impact Test Simulations

Numerical simulations of the Taylor rod-on-anvil impact tests were performed using AUTODYN employing an axisymmetric model created for simplification of the projectile and a block of quasi-rigid steel for the anvil, as shown in Figure 14. For the projectile, a quarter cylinder of radius 3.81mm and length 30mm was created. The projectile was given an initial velocity of 250m/s and 155m/s in two simulations, equal to the experimental velocities of the Al 6061 and OFHC Cu, respectively. A boundary condition of zero velocity was applied to the nodes on the back face of the steel anvil. Refinement of the finite-element mesh and a lower-K graded mesh were used to increase the fidelity near regions of the simulation that undergo high strain while providing a coarser mesh elsewhere in the model to minimize computation time. To record the deformation profile of the cylinder an array of gauge points was created along the length of the projectile at the top edge. These gauge points provide the coordinates needed to plot a profile of the deformed simulated sample cross section. Figure 15 shows examples of the deformed state simulations for both aluminum and copper rod-shaped samples impacting the quasi-rigid steel anvil.
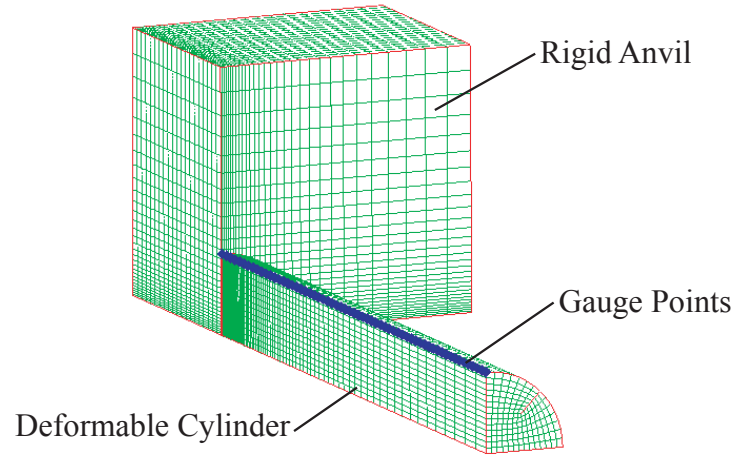
Figure 14: Taylor rod-on-anvil impact test AUTODYN simulation. Rod-shaped samples of the deformable material impact the quasi-rigid steel anvil.
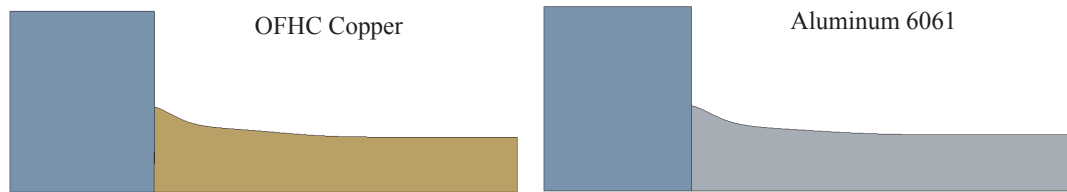
Figure 15: Deformed state profiles for simulated samples for the Taylor rod-on-anvil impact test.

4.2   Material Models

A variety of material constitutive strength models are available for simulations in ANSYS AUTODYN's material library. Comparisons were made between the predictions of the Johnson-Cook and Steinberg-Guinan strength models, as these two are most relevant to fcc metals such as aluminum and copper. The Zerilli-Armstrong model has been shown to be more applicable for bcc metals and hence, was not considered in the present work. It was found that the Steinberg-Guinan model gave less accurate predictions of the deformation states and was more difficult to modify precisely. Instead the Johnson-Cook strength model was used for studying the high strain-rate deformation response of Al 6061 and OFHC Cu. The empirical model includes isotropic strain hardening, strain rate sensitivity, and thermal softening [26] and is expressed as,

$$\sigma = (\sigma_y + B\epsilon^n)(1 + C\ln\dot{\epsilon}^*)(1 - T^{*m}) \tag{6}$$

where $\dot{\epsilon}^*$ and T^* are the normalized strain-rate and temperature, respectively, with material constants σ_y, B, C, n and m. Constants B and n represent the effect of strain hardening, and the constants C and m represent the effects of strain-rate and temperature, respectively. Three model parameters were found to cause the most significant change when varied to correlate the simulated deformation profile to the experimentally obtained profile: the yield stress, σ_y, strain-rate constant, C, and the hardening constant, B. The constants obtained from the correlation of simulations with Taylor rod-on-anvil impact experiments performed on aluminum and copper rods were then used to design the geometries of the 7.62 and 80mm gas gun hollow concentric die setup and predict the deformation response.

4.3   Die Design Considerations

An important consideration for the design of the hollow concentric die was to establish the die angle, which determines the magnitude and depth of stress-strain dissipation in the aluminum rod accelerating through the copper die. Increasing die angle increases both the magnitude of the longitudinal stress component and the depth of strain propagation. Decreasing die angle limits the strain propagation to the interface, but also lowers the

magnitude of the strain. Simulations performed using AUTODYN revealed that a die taper angle of 5° would provide the best range of the extent of strain and its localization for creating a well defined interface layer based on the properties of aluminum and copper and for the range of velocities that can be explained in the present work. All subsequent numerical simulations were then performed for design of the hollow dies for use with the 7.62 and 80mm gas guns to investigate the extent and depth of strain in the aluminum rod and copper die over a range of velocities up to 900m/.

4.4 Gas Gun Concentric Die Simulations

To model the acceleration of an aluminum rod through concentric copper die in AUTODYN, a quarter symmetry 3D model was used featuring a hollow cylinder with a tapered inner surface to replicate the die geometry. Boundary conditions were applied to the nodes along the back surface of the die, those in contact with the catch tank, to restrict axial motion and to nodes along the outer surface, those in contact with the steel housing, to restrict radial deformation. An array of gauge points was added to the top edge of the aluminum cylinder to measure displacement along the surface throughout the simulation. The distance from the exit end of the die to the tail end of the projectile was used to correlate the AUTODYN simulation results with the samples recovered from experiments. Figure 16 shows an example of the simulation setup for the 7.62mm gas gun geometry.
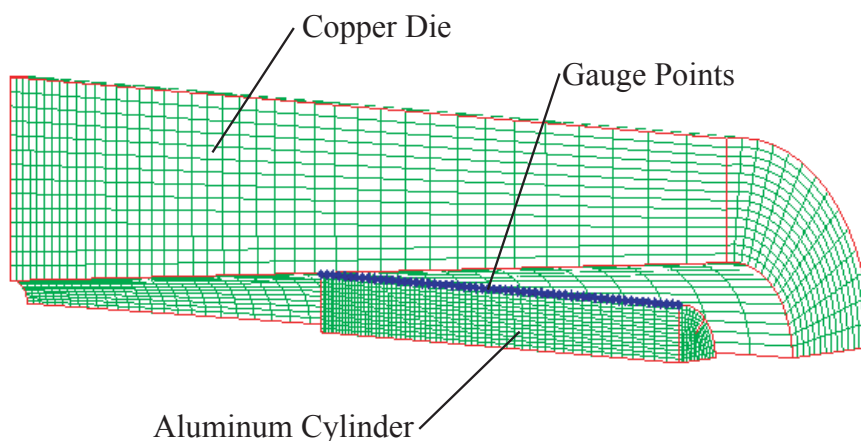
Figure 16: AUTODYN setup of 7.62mm gas gun concentric die simulation. Aluminum cylinder passes through hollow tapered die.

For material models, the modified versions of Al 6061 and OFHC Cu validated using the Taylor rod-on-anvil impact tests were used. In the experiment, portions of the aluminum cylinder were extruded through the die to the point of fracture. To account for this, erosion control was added to the material model for aluminum based on a plastic strain limit. A graded mesh was used for the cylinder to both increase the fidelity of the simulation in areas of higher strain and also to minimize computational time.

Simulations were also performed to design the 80mm gas gun experiments involving different die geometries and higher velocities. The first design featured the die with constant 5° tapered hole. This was chosen to match the characteristics of the 7.62mm gas gun concentric die simulations and to study directly the effects of increased velocity. For the simulation in AUTODYN, an initial velocity of 915m/s was given to the aluminum projectile while no boundary constraints were applied to the die and housing. The setup and mesh for the constant taper simulation are shown in Figure 17.
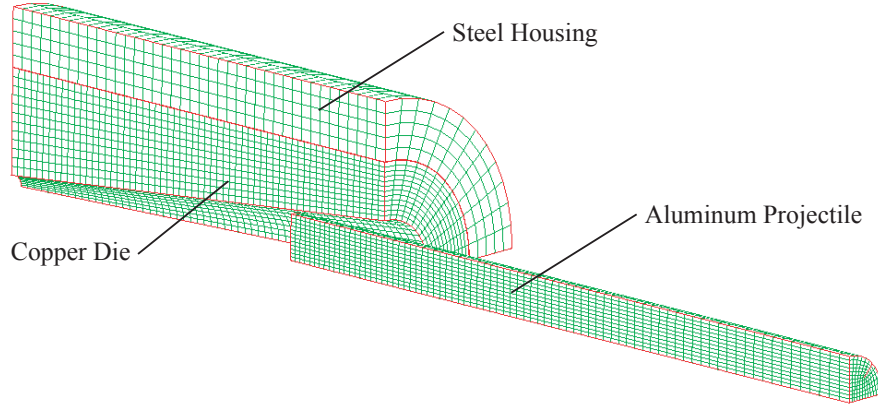
Figure 17: AUTODYN simulation of 80mm gas gun constant taper concentric die.

Results from the constant taper simulation show the propagation of strain throughout the entire cross section of the aluminum projectile. Large deformation was also observed at the exit of the die. A contour plot showing plastic strain for the simulation at $48\mu s$ is shown in Figure 18. It can be seen that the strain varies from 104% along the axis to 130% at the outer edge in the region close to the exit.

Another simulation was performed using a hybrid die geometry incorporating first a

23
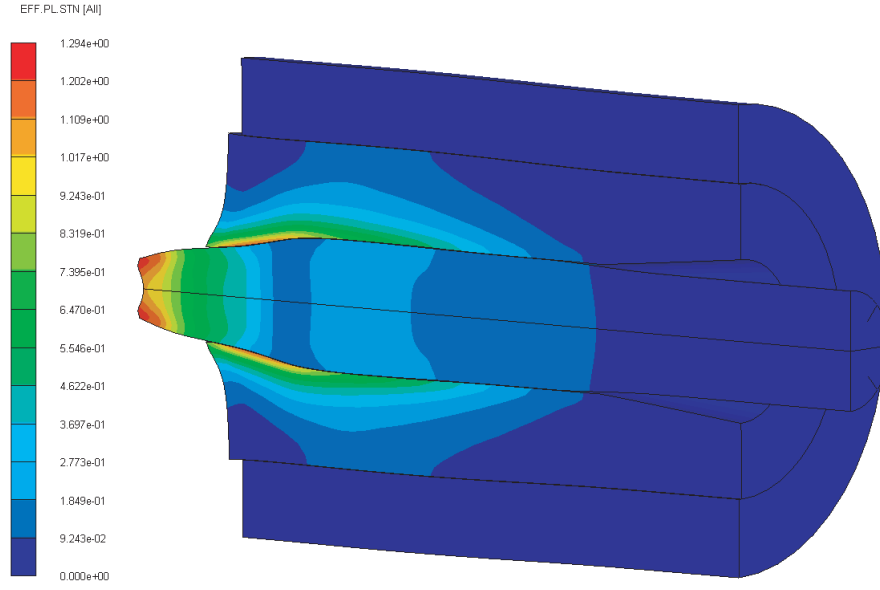
Figure 18: Strain contour plot of 915m/s constant taper die at 48μs.

5° tapered hole for 30mm of die length. For the remaining 10mm length a constant cross sectional hole of diameter 5.12mm was chosen to deform only the outer 1.25mm of the aluminum cylinder. Figure 19 shows the initial setup and mesh for the hybrid die geometry simulation. Nodes along the interface of the tapered and constant hole segments were joined.
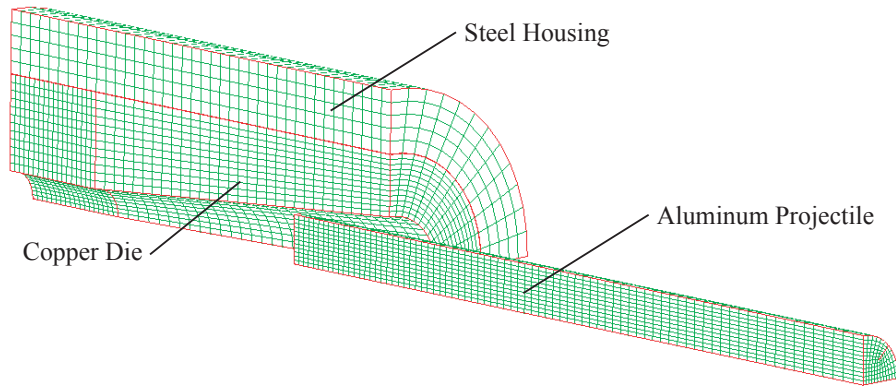
Figure 19: AUTODYN simulation of 80mm gas gun hybrid taper concentric die.

A strain contour plot of this simulation at 30μs, illustrated in Figure 20, shows strains of 104% in the tip of the aluminum. Strain is also being localized along the surface of the

aluminum. Giving a radial dependance that is more defined than the strain contours shown in Figure 18.
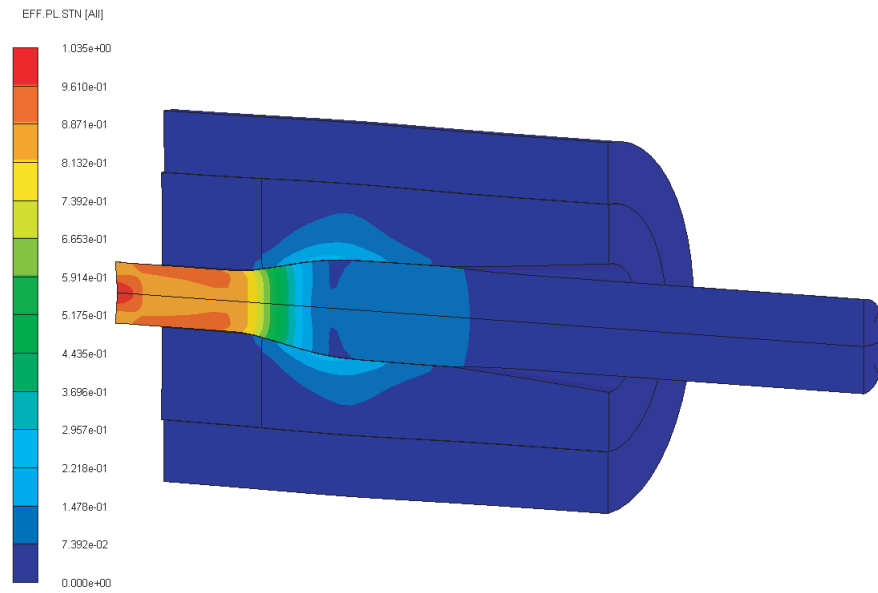
Figure 20: Strain contour plot of 915m/s hybrid taper die at 30μs showing higher surface strain in aluminum.

CHAPTER V

RESULTS AND DISCUSSION

Results for the Taylor rod-on-anvil test are presented first to show the validation of the simulation strength model parameters. The different parameters, their effects on the deformation profile, and final values that gave the best correlation with experimental observations are given. Validation of the concentric die design is presented next with simulation outputs for the strains in the copper die and aluminum rod. The simulation is compared to experimental results by measuring the depth of the projectile in the die and including erosion control to obtain a more realistic fracture model. Analysis of the interface friction and wear effects is shown in microstructural characterization of the interface region including scanning electron microscope images combined with energy dispersive spectroscopy. Mircohardness measurements were also performed to study the regions around the interface.

5.1   *Material Model Validation Based on Rod-on-Anvil Impact Tests*

Aluminum and copper samples from the Taylor rod-on-anvil impact tests were recovered, shown in Figure 21, and their final deformation states measured. The cross section profile of the recovered impacted samples were recorded using the optical comparator for comparison with the simulation gauge point data. These profiles allowed the Johnson-Cook strength model parameters in the constitutive equations to be varied while studying their effects on the resulting deformation. Two characteristics of the deformation were most significant when fitting the profiles, both the deformation foot print of the impact face and the propagation of deformation throughout the length of the cylinder. It was found that the strain rate constant, C, gave the most control over the amount of deformation at the impact face, as shown in Figure 22a. The hardening constant, B, also had a small, more localized effect on the impact face. The other significant parameter was the yield stress, σ_y, which determined the propagation of deformation along the length of the cylinder and any barreling effects, illustrated in Figure 22b. This is not unexpected and is typical for observations of

fcc metals [28].

Figure 21: Final deformation states for recovered copper and aluminum samples from the Taylor rod-on-anvil impact tests.

The yield stress, strain rate constant, and hardening constant were modified to achieve the best correlation between the experimental profiles of the final recovered deformation state and simulation results for Al 6061 and OFHC Cu, shown in Figure 23. The correlation was based on two criteria for validation, namely the final impact-end diameter and overall length of the recovered samples which are listed in Table 1. With the use of three Johnson-Cook strength model parameters, σ_y, C, and B, listed in Table 2, the simulation results were matched with the experimental data within 2%. It should be noted that the adjusted strength parameters are different from the original values, due to differences in the processing history of the aluminum and copper materials used in the present work.

Table 1: Final deformation state criteria dimensions for recovered Al 6061 and OFHC Cu samples and simulation results with associated error.

Material		Length [mm]	Error [%]	Diameter [mm]	Error [%]
Al 6061	Exp	25.77	-	11.32	-
	Sim	25.81	0.15	11.52	1.78
OFHC Cu	Exp	25.20	-	11.58	-
	Sim	25.05	0.58	11.68	0.91

a)

250 m/s Al Profile - Strain Rate Constant

b)

250 m/s Al Profile - Yield Stress
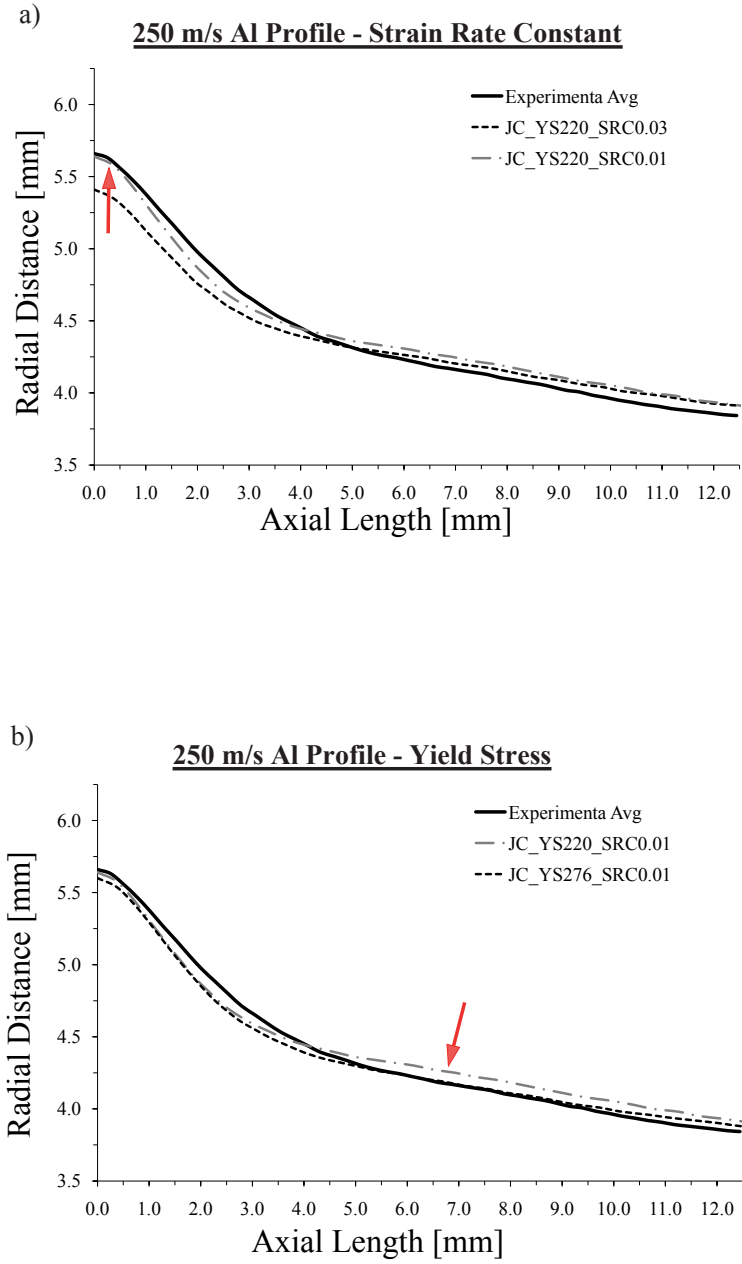
Figure 22: a)Decreasing the strain rate constant, C, the deformation at the impact face was increased. b)By increasing the yield stress, σ_y, the deformation did not propagate as far along the length of the sample.

Al 6061 at 250 m/s

OFHC Cu at 155 m/s
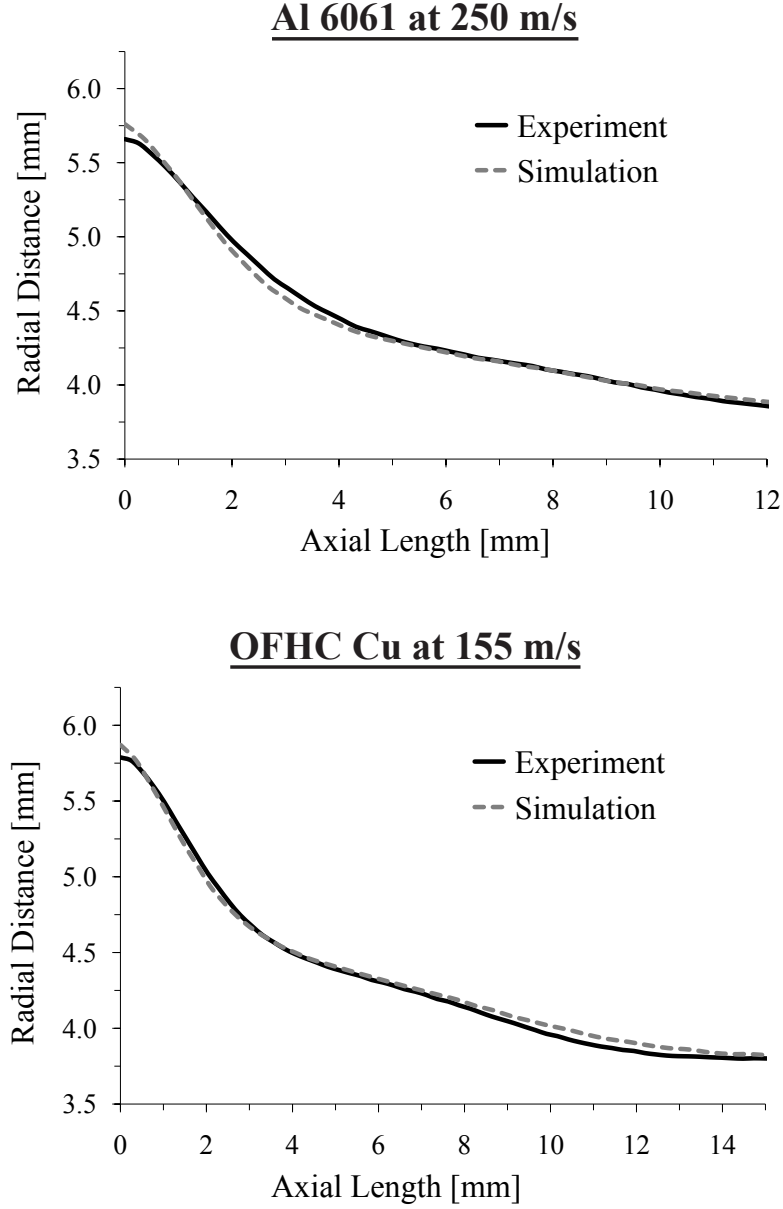
Figure 23: Final correlation between the experimental profiles of the final recovered deformation state and simulation results for Al 6061 and OFHC Cu based on adjusted coefficients of strength model listed in Table 2.

Table 2: Original and (Adjusted) Johnson-Cook model parameters.

Parameter	σ_y [MPa]	C	B [10^5 MPa]
Al 6061	220 (276)	0.03 (0.01)	4.26 (3.8)
OFHC Cu	140 (310)	0.025 (0.01)	2.9 (2.9)

5.2 Concentric Die Design Simulation

Concentric die design simulations were performed to predict the strain developing at the Al-CU interface regions following validation with experiments. In order to match the concentric die simulations with experimental results, the length of the projectile remaining in the die was measured from the exit end of the die to the tail end of the projectile. The validated Johnson-Cook strength model with the fitted constants for Al 6061 and OFHC Cu obtained from the Table 2 were used. However, in the experiment performed at 700m/s, part of the aluminum cylinder strained significantly, and fractured as shown in Figure 10. This was accounted for in the simulations by adding plastic strain erosion to the material model for aluminum. As elements in the simulation reach a specified control strain value they are deleted and their momentum no longer retained. This helped reduce the velocity of the aluminum projectile to obtain the correct penetration depth into the copper die. The depth was measured and compared to simulations for the 500 and 700m/s samples. By controlling the erosion strain in each simulation, ranges of acceptable strains were found that provided good matching at both velocities, as shown in Figure 24. For the 500m/s experiment lower erosion strain values produced more accurate results until the value became so low that the sample fractured unrealistically. In the 700m/s case increasing the erosion strain reduced the error asymptotically. While the erosion strain does not appear to have a significant effect on the penetration depth it is important to note its effects and obtain the more realistic fracture model. Figures 25 and 26 show the strain contour in both the aluminum projectile and copper die for the 500 and 700m/s experiments at various times. Maximum strains experienced in the aluminum at the interface as it exits the die are 143% and 155% for the 500 and 700m/s experiments, respectively. The copper die also shows increased strain with velocity, from 6.5% to 15%. Erosion control strain causes portions of the aluminum to fracture after exiting the die.
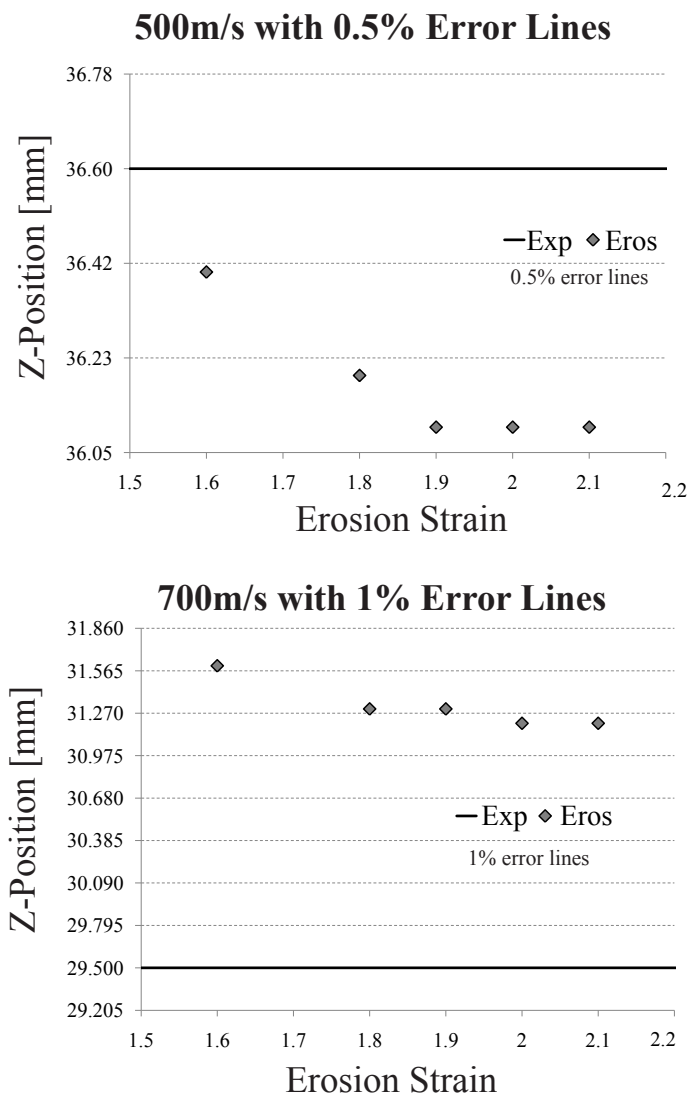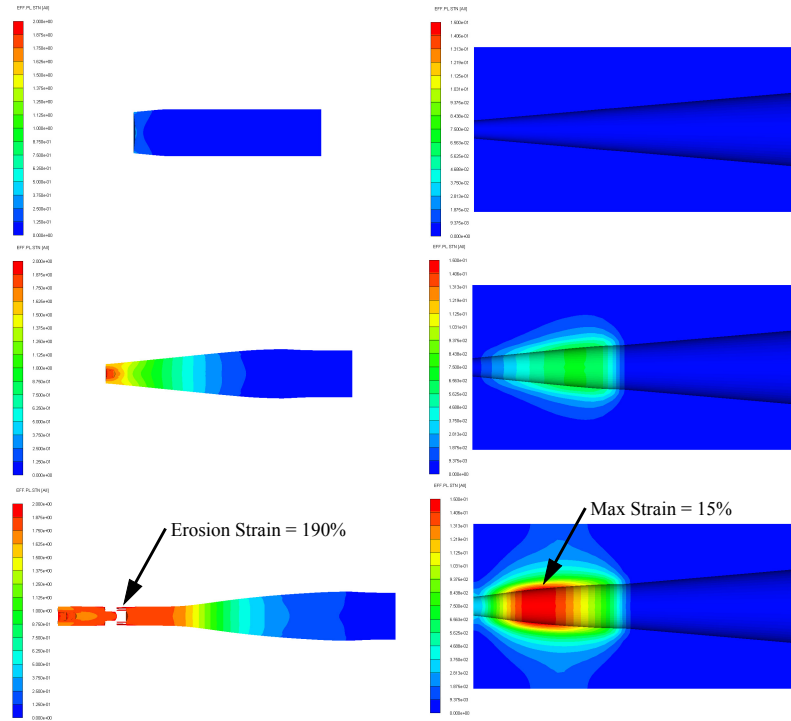
Figure 24: Depth of projectile remaining in die for different erosion strains at each velocity.
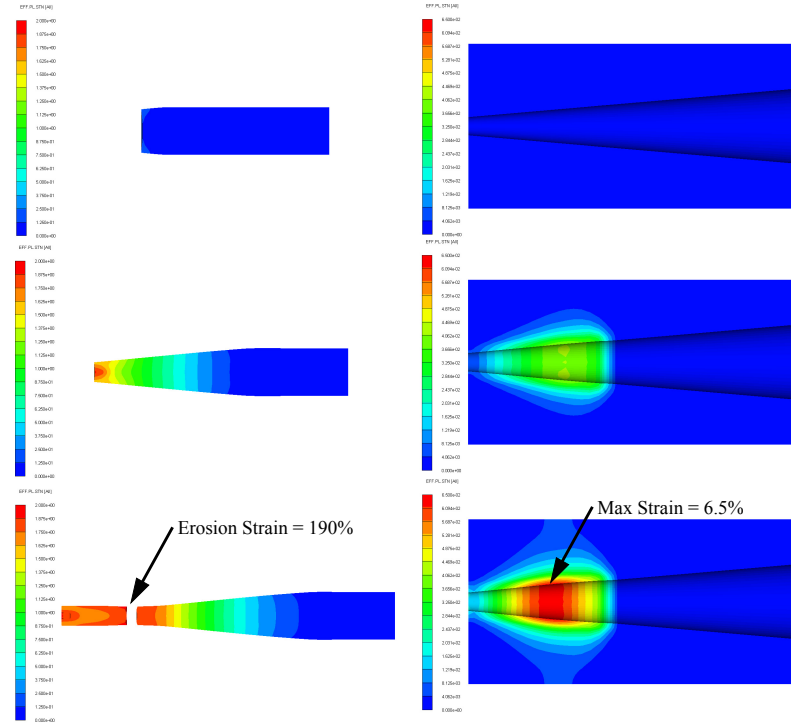
Figure 25: Strain contour plot for aluminum projectile and copper die of 500m/s experiment at 8, 36 and 52μs with erosion strain of 1.9.

Figure 26: Strain contour plot for aluminum projectile and copper die of 700m/s experiment at 8, 26 and 40μs with erosion strain of 1.9.

5.3   Analysis of Interface Friction and Wear Effects

Dies for both the 7.62 and 80mm gas gun concentric die experiments were sectioned and microstructural analysis was performed to help characterize the interface region and any layer deposits. An optical microscope was used for qualitative descriptions of the layer while a scanning electron microscope (SEM) combined with energy dispersive spectroscopy (EDS) were used to better characterize the composition. Microhardness measurements were also performed in regions close to and in the interface layer to obtain an understanding of phase changes along the interface region.

5.3.1   Microstructural Characterization of Interface Layer

Rod-shaped aluminum samples accelerated through hollow concentric copper dies at 250, 500, and 700m/s in the 7.62mm gas gun were used to study the effect of velocity on the interface region. Images were recorded using the optical microscope at various magnifications to observe the continuity and measure the thickness of the interface layer. At 250m/s a discontinuous interface layer of up to 5μm thickness, with some alloying was observed. Figure 27 shows images of the 250m/s interface layer of two different regions.
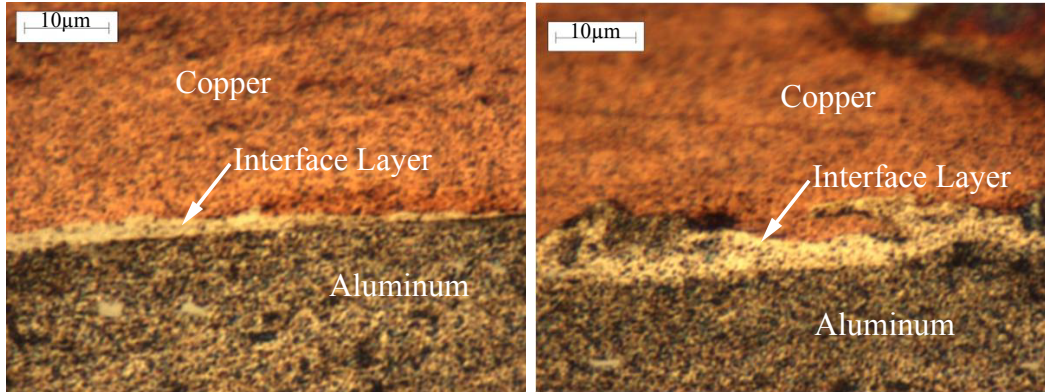
Figure 27: Optical microscope images of regions of interface layer for 250m/s experiment.

For the 500m/s sample a discontinuous interface layer was still observed but with a thickness of the order of 20-30μm, as seen in Figure 28. A more continuous layer was found in the 700m/s sample, with thickness of 30-50μm along longer portions of the interface. Images of this alloy layer are shown in Figure 29.
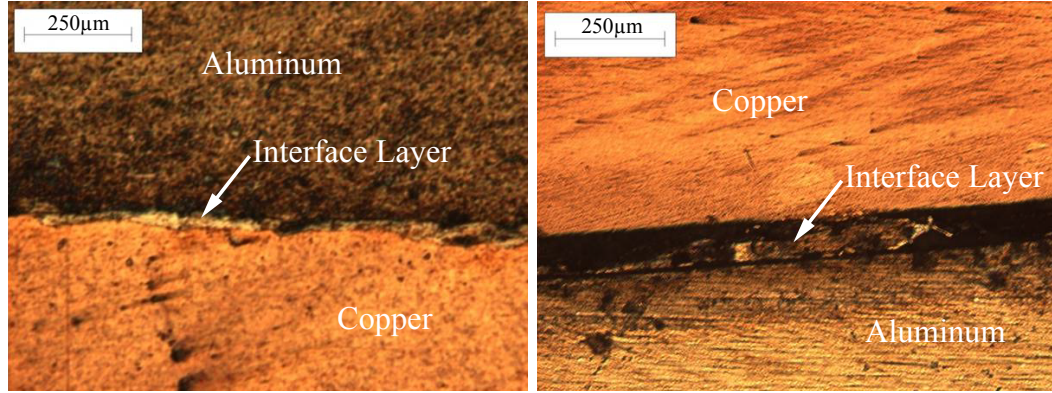
Figure 28: Optical microscope images of regions of interface layer for 500m/s experiment.
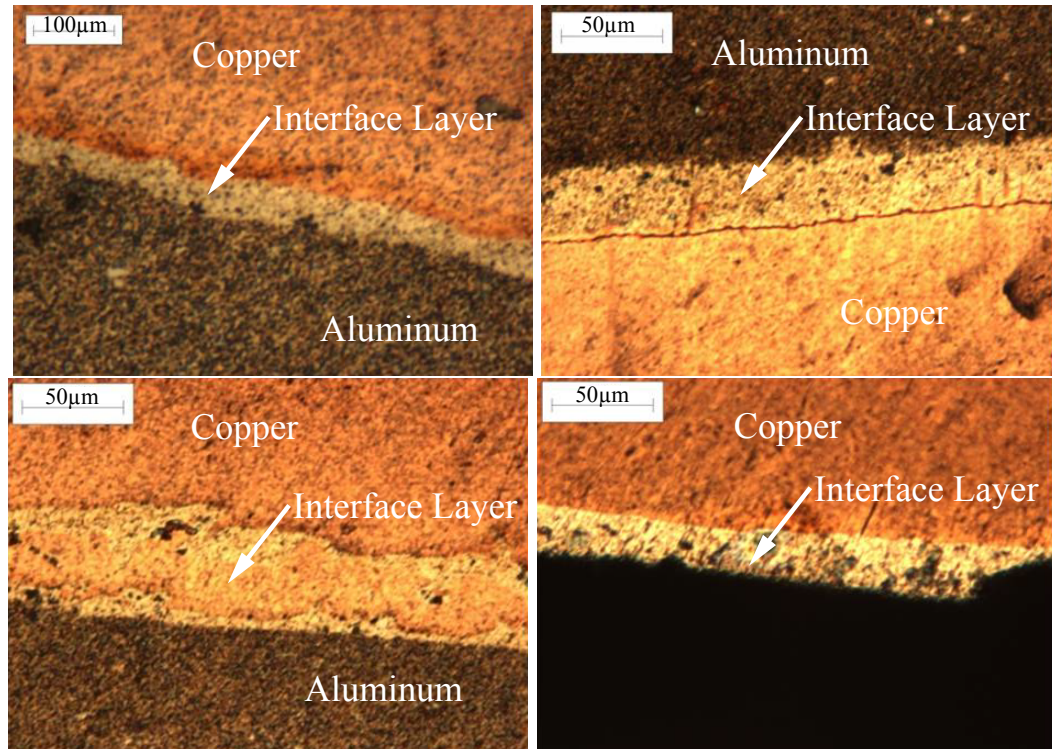
Figure 29: Optical microscope images of regions of interface layer for 700m/s experiment.

For the concentric die experiments using the 80mm gas gun the aluminum projectile did not remain embedded in the copper die. A layer of deposited aluminum was still observed along the interface region but only in certain areas, possibly due to lack of alignment which may not have been as accurate as the 7.62mm gas gun resulting in projectile orientation variations, and nonuniform interface layer. However, in the constant taper die setup the layer was significantly thicker, on the order of 80μm, as shown in Figure 30 for 880m/s.
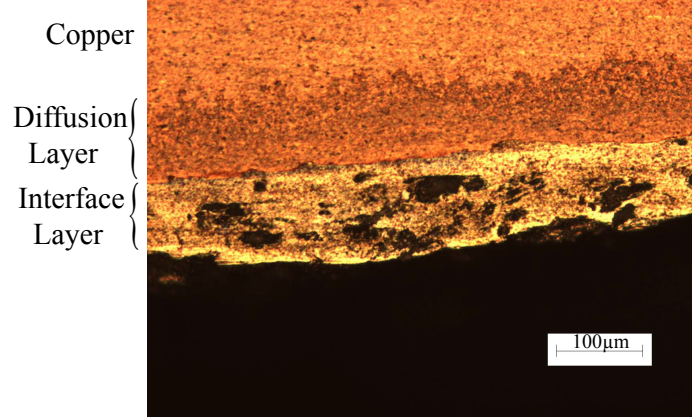
Figure 30: Optical microscope image of interface layer for 880m/s constant taper die.

Results for the hybrid die experiment were less conclusive. A thin layer of approximately 20μm was observed and only at a few locations along the length of the interface region. Figure 31 shows one such deposit for the 915m/s hybrid die experiment.
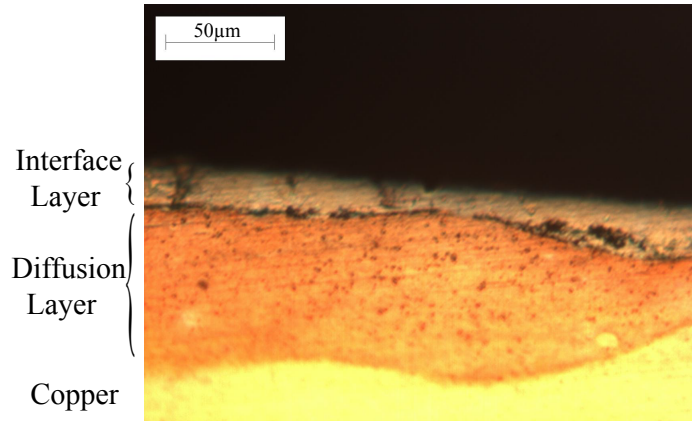
Figure 31: Optical microscope image of interface layer for 915m/s hybrid taper die.

Scanning electron microscopy (SEM) was performed to record high magnification images of the interface layer. In the 700m/s 7.62mm gas gun experiment, it was possible to resolve the microstructure of the interface layer, as seen in Figure 32. The presence of equiaxed grains of $\approx 3\mu$m size and lack of any cellular/dendrite structure suggests solid-state alloying in the interface layer. EDS was used to determine the chemical composition of the interface layer areas in the 700m/s sample. Spectral analysis (box scanned areas) shows the distinct aluminum and copper materials on the respective sides, and an aluminum-rich alloy of aluminum in the interface layer, as illustrated in Figure 33.
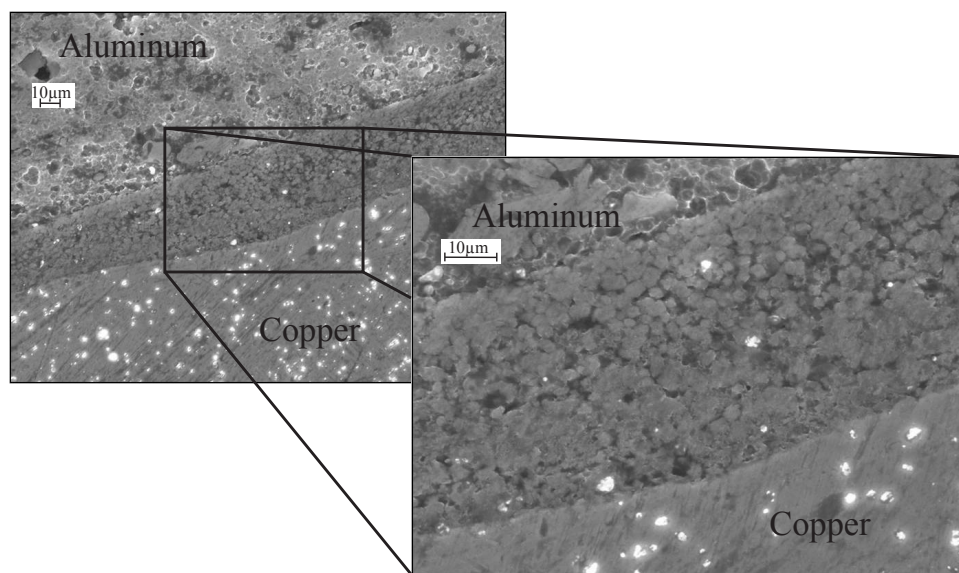
Figure 32: SEM image of grain structure for interface layer in 700m/s sample.
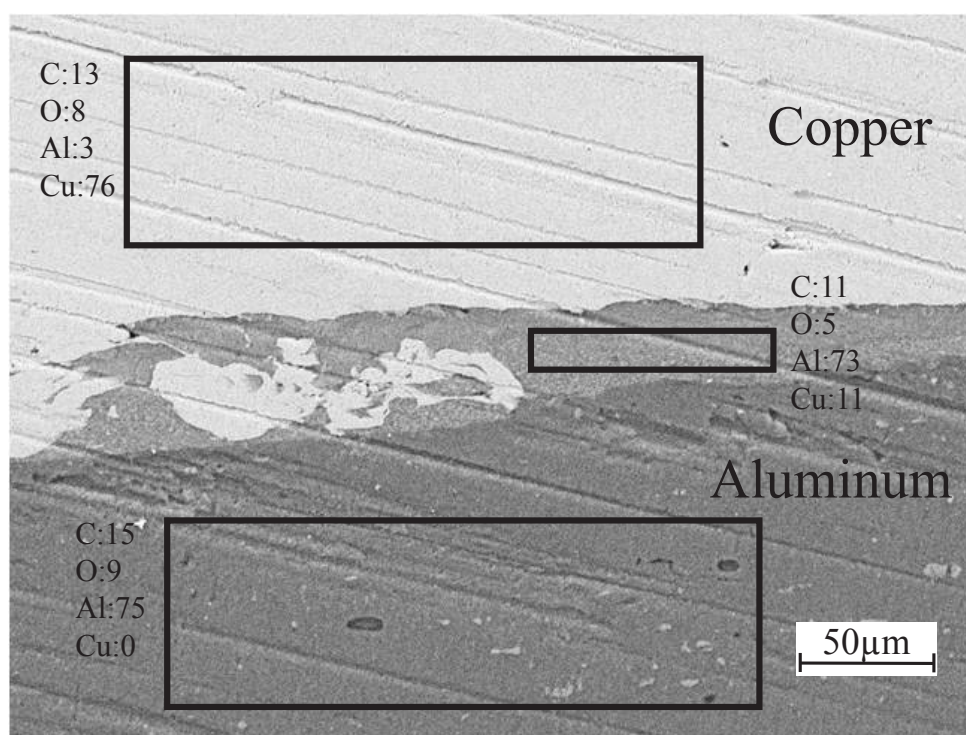
Figure 33: EDS box scans of 700m/s concentric die experiment. Values for the copper die, aluminum projectile, and interface region are given.

High magnification SEM images of the 80mm gas gun samples revealed a similar interface layer of melted and re-solidified aluminum deposited along the surface of the copper die shown in Figure 34. EDS scans of the polished interface layer show the quenched deposit layer to consist of primarily aluminum with impurities and negligible copper, while the die region contains primarily copper and under 5% aluminum (possibly impurity left over from polishing compound). In the region of the copper die adjacent to the aluminum layer a mixing of aluminum and copper was observed (Cu-42% and Al-48%). The mixed layer is believed to be formed due to diffusion between the melted aluminum and the copper die, which is unlike the alloy layer formed due to solid-state alloying in the lower velocity experiments.
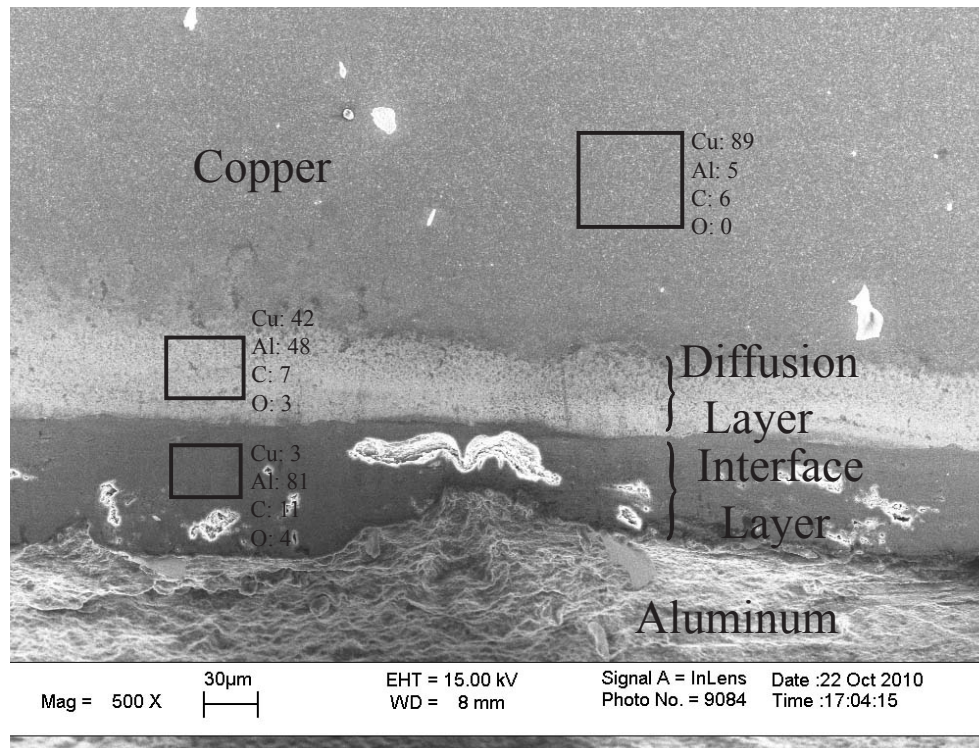
Figure 34: EDS box scans of three regions in the 880m/s constant taper die design: a layer of quenched aluminum, the copper die, and mixed region near the deposit layer.

5.3.2 Microhardness Measurements

To better study the interface layer formed in the 7.62mm gas gun concentric die experiments microhardness measurements were performed in regions within and adjacent to the interface. Mappings were made through the copper die, interface layer, and aluminum projectile. Average values for the Vickers hardness of aluminum and copper near the interface layer were recorded as 136HV25 and 114HV25 respectively. As the indenter was moved closer to the interface some softening was observed. However, on the interface layer itself a much higher hardness value of 205HV25 was recorded. The higher hardness value indicates solid-state alloying occurring due to severe plastic deformation, which is consistent with the presence of equiaxed grains of Cu-Al alloy in the interface layer, rather than just melted and re-solidified aluminum. Figure 35 shows the mapping of the indent locations, with the indent '4' localized in the interface layer. The values at these locations are shown in Figure 36.

Microhardness measurements were also performed on the constant taper and hybrid die designs in regions of the copper die near the interface. Figure 37 shows a mapping of the indent locations in the 880m/s constant taper die. The hardness values were seen to increase as the measurements were taken closer to the interface region, as shown in Figure 38. The increase in hardness value of the copper die is a result of work hardening. Low hardness in the layer is expected from the formation of melted and re-solidified aluminum.
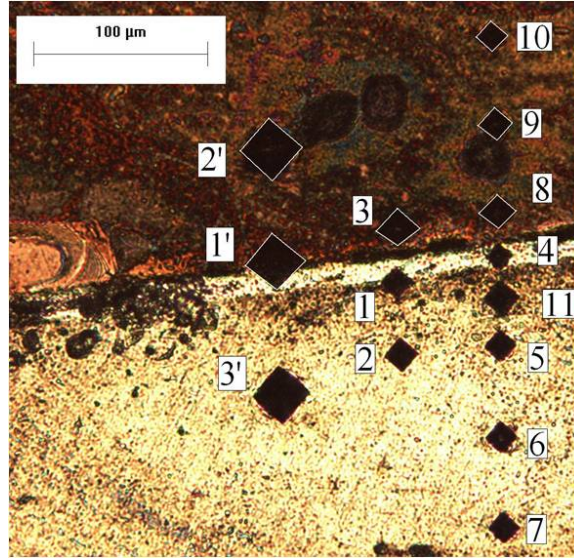
Figure 35: Map of microhardness indentation locations for the 700m/s concentric die design. Right most measurements are plotted in Figure 36.
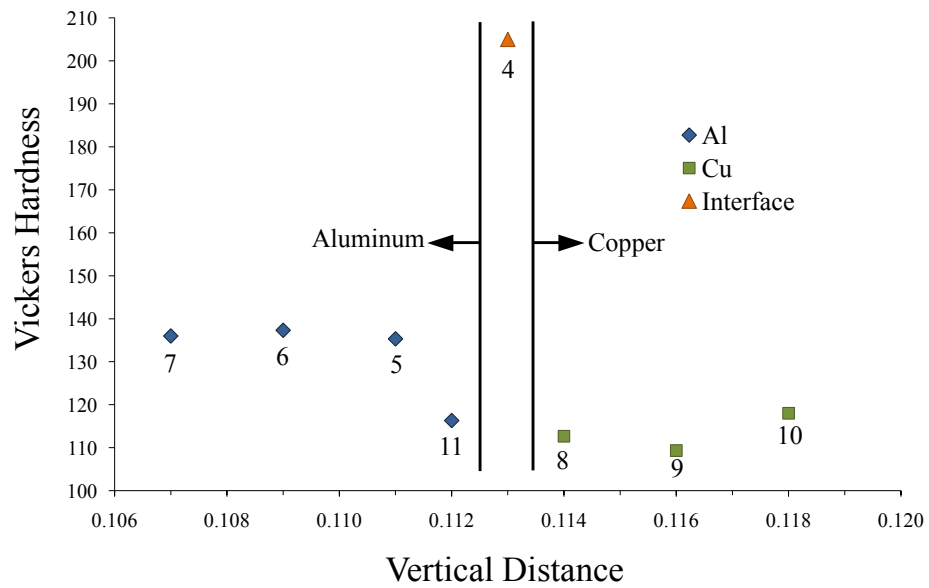
Figure 36: Microhardness values for 700m/s sample. Interface layer displays higher hardness than either aluminum or copper due to solid-state alloying. Numbers correspond to indenter locations in Figure 35.
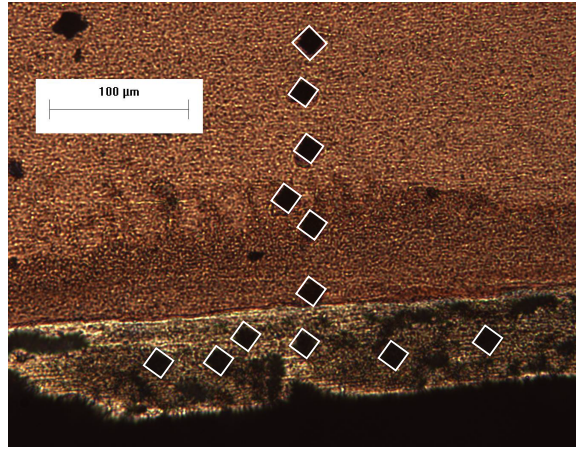
Figure 37: Map of microhardness indentation locations for the 880m/s hybrid taper concentric die design.
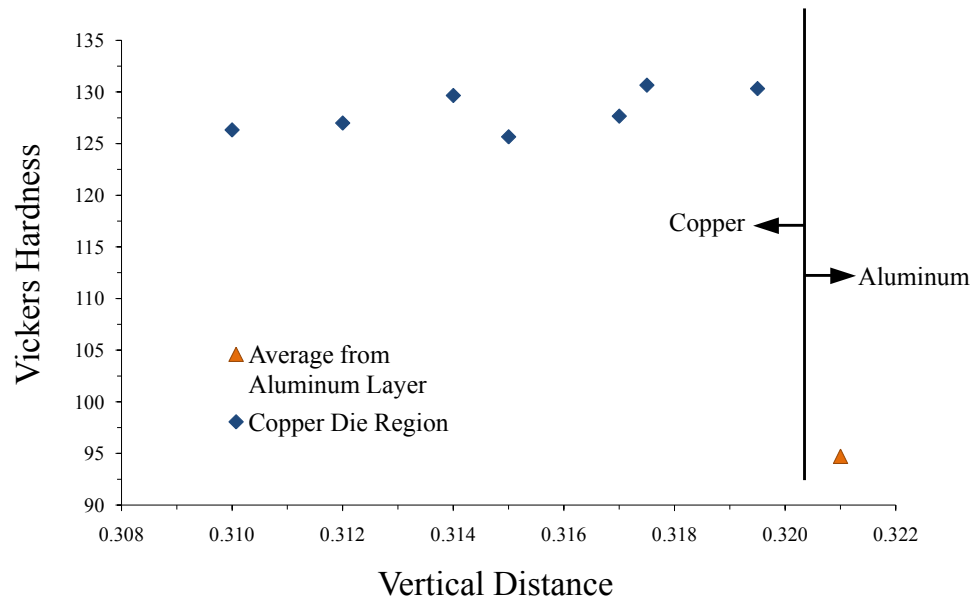
Figure 38: Microhardness measurements for 880m/s sample. Hardness values increase as measurements are taken closer to the interface, due to work hardening.

5.3.3 Interface Characteristics Correlated with Armature-Rail Wear Effects

In this work experiments have been designed to investigate the use of gas gun systems to study interface wear effects by accelerating rod-shaped samples of aluminum through hollow concentric dies of copper. An application where such effects of high-strain-rate loading and dynamic friction are important is associated with armature-rail interaction during railgun operation. Numerical simulations performed with the geometries and conditions employed in the experiments conducted in the present work predict increased stress-strain localization along the interface for experiments performed at higher velocities. The hybrid die design simulations particularly show that the die geometry allows for a strain profile with higher surface strains localized along the interface in the aluminum, in spite of the smaller overall reduction in the cross-sectional area. Analysis of the microstructure of the interface illustrates solid-state alloying in the lower velocity range, at velocities up to 700m/s, as evidenced by small, equiaxed grains and high hardness values. At velocities greater than 800m/s, observations show the melting and re-solidification of aluminum along the interface. Figure 39 shows a comparison of the interface layer in the case of the experiments at 500, 700, and 880m/s. The interface layer in the 500m/s experiment has equiaxed grains of Al-Cu alloy on the order of 3-4μm, which decrease to 2-3μm size in the case of the interface layer at 700m/s. On the other hand, the interface layer observed in the 880m/s experiment indicates the re-solidification of a melted almost pure aluminum layer with grain size of 0.25μm. EDS results indicate diffusion between the melted aluminum layer and the copper die, in the case of the higher velocity experiments.

Experimentation with the gas gun systems and corresponding simulations give a range of velocities over which interface wear effects associated with high velocity sliding of aluminum across a copper die can be studied. Interface characteristics incorporating both solid-state alloying and melting and re-solidification of aluminum are achieved as a function of velocity. The key differences in the loading conditions and interface layer characteristics are highlighted in Table 3. It can be seen that based on the die geometry and corresponding velocity of the accelerating aluminum projectile through the tapered continuous and hybrid dies, the bulk and interface strains vary with strains localized along the interface substantially

41

increasing with increasing velocity. The strain localization in turn influences the characteristics of the interface layer, with severe plastic deformation creating an alloy layer (of few micron grain size) formed due to solid-state alloying between copper and aluminum at velocities of 500 and 700m/s and interfacial melting forming a melted and re-solidified aluminum layer (of sub-micron grain size) in the case of the 880 and 915m/s experiments. Correspondingly, the microhardness values of the interfacial regions are likewise influenced with the layer of much higher hardness formed due to solid-state alloying of copper and aluminum, in contrast to the interface layer consisting of simply melted and re-solidified aluminum. Additional experiments employing the hybrid copper die, with varying taper angles can provide further variation in the degree of interface strain localization without significant bulk deformation, to evaluate the structural characteristics and mechanical properties of the resulting interface layers. The work conducted demonstrates the applicability of gas gun methods to study such interface wear during acceleration of aluminum rod through a hollow copper die resulting in differences in interface structure as a function of velocity and die design.
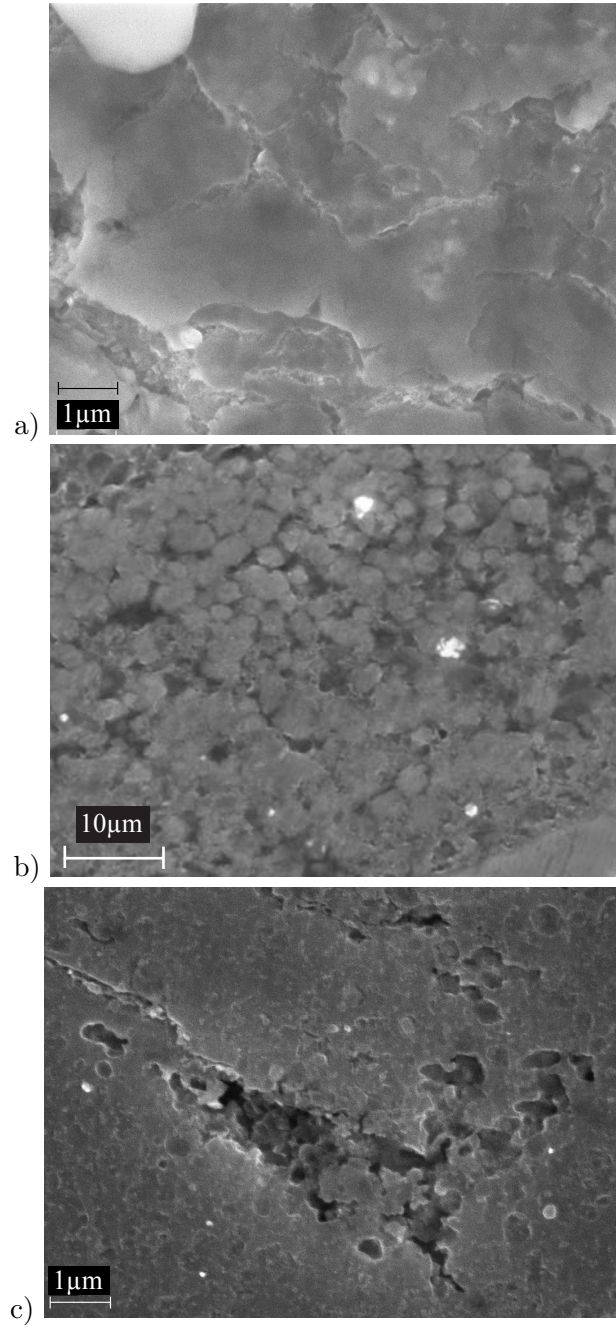
Figure 39: Interface layer grain size for a)500, b)700, and c)880m/s experiments.

Table 3: Key differences in loading conditions and interface characteristics.

Velocity	250m/s	500m/s	700m/s	880m/s	915m/s
Geometry					
Gunsystem	7.62mm	7.62mm	7.62mm	80mm	80mm
Die Design	5° Taper	5° Taper	5° Taper	5° Taper	5° Taper
	Continuous	Continuous	Continuous	Continuous	Hyrbid Die
Entry ⌀	13.7mm	13.7mm	13.7mm	10mm	10mm
Exit ⌀	3.18mm	3.18mm	3.18mm	3.3mm	5.12mm
Areal Reduction	82.6%	82.6%	82.6%	81.2%	54.9%
Load Conditions					
(Max Strain)					
Al Interface	-	143%	155%	210%	193%
Al Bulk	-	142%	152%	189%	172%
Cu Interface	-	6.5%	15%	155%	46%
Cu Bulk	-	0%	0%	15%	10%
Interface					
Characteristics					
Continuity	Discontinuous	Discontinuous	Continuous	Continuous	Continuous
Thickness	5μm	20-30μm	30-50μm	80-100μm	20-30μm
Structure/ Composition	Alloyed w/ equiaxed grains	Alloyed w/ equiaxed grains	Alloyed w/ equiaxed grains	Melted and re-solidified	Melted and re-solidified
Grain Size	-	3-4μm	2-3μm	0.25μm	-
Microhardness	-	-	204HV0.25	95HV0.25	-

CHAPTER VI

CONCLUSIONS AND FUTURE WORK

6.1 Concluding Remarks

The objective of this work has been to investigate the applicability of the gas gun to study the characteristics of interface wear during acceleration of an aluminum rod through a hollow copper wedge. The study of such wear characteristics is important in applications such as during armature-rail interaction in railgun operation. The approach involved developing coefficients of constitutive strength models for aluminum 6061 as well as oxygen-free high-thermal conductivity copper. Taylor rod-on-anvil impact tests combined with numerical simulations were performed to validate and create reliable constitutive strength models for armature (aluminum) and rail (copper) materials. The validated models were then used to design concentric die experiments and predict stress-strain conditions associated with acceleration of armature through hollow concentric copper die. These simulations were then used in tandem with gas gun experiments over a range of velocities to study the armature-rail interface wear effects encountered in a rail-gun operation.

The Taylor test method is a well documented approach to studying a material's response to dynamic, high strain-rate conditions. These results were used with the Johnson-Cook strength model is ANSYS AUTODYN to give simulation results of the cross section profiles for comparison to experimental samples. Predictions of the impact face deformation and overall length were within 2% of experimental observations.

The fitted material strength models were then used to create a simulation of the concentric die experiment for the 7.62mm gas gas gun. Simulation results were compared with the sectioned specimens from the experiments. By adding erosion control to the material models, a more realistic behavior of the aluminum, including fracture, was developed. Experiments for the 80mm gas gas gun system were developed to achieve higher velocities and study the effects of different die configurations. The previously developed material models

were used to create simulations to observe expected deformation, study strain propagation, and compare die geometries.

Analysis of the interface region was performed on the recovered die experiments to characterize any interface layer. Optical microscope images gave an indication of the thickness and continuity of the observed interface layer. For the 7.62mm gas gun shots this layer was seen to both thicken, from 5-50μm, and increase in its continuity from discontinuous deposits in the 250 and 500m/s experiments to more continuous layer at 700m/s. Microhardness measurements indicated a higher hardness value at the interface and SEM images were able to resolve the microstructure, confirming smaller grain sizes in the interface that would produce these values. EDS of the interface layer revealed an aluminum-rich alloy as a result of solid-state alloying. Results for the 80mm gas gun experiments revealed a different type of interaction. While a thicker deposited layer, on the order of 80μm, was observed, it appeared to be a result of molten aluminum being re-solidified along the surface of the copper die. Alloying in the copper die near the deposited layer is a result of diffusion between the molten aluminum and solid copper die. These results show that the gas gun systems provide an experimental setup to test a range of velocities that include both solid-state alloying of the aluminum projectile and copper die as well as melting of the aluminum in the interface. Similar variations have been reported in the case of armature-rail interface characteristics although under more extreme conditions.

6.2   Recommendations for Future Work

This work was designed to investigate and understand the interface wear characteristics associated with acceleration of an aluminum rod through a hollow copper die. Numerical simulations with validated material models allow for die geometries to be designed to achieve a range of strains (local and bulk) that result in solid-state alloying due to severe plastic deformation localized at the interface, at velocities below 800m/s, and melting, re-solidification, and diffusion of aluminum at the copper die interface at velocities above 800m/s. Future work needs to incorporate the C180 alloy of copper which has higher strength and unknown high-strain-rate response. The effects of the hybrid die design at varying velocities also

needs to be evaluated. Another element of interest would be to include the effect of Joule heating at the interface. A reverse configuration in which the die is fired at a stationary aluminum cylinder may be required to allow for heating of the aluminum in the experiment chamber. With the versatile methods and models developed in this research these different materials and configurations can be better explored by future studies, employing the gas gun at velocities in the range of 200-1200m/s.

REFERENCES

[1] Elder, D. *IEEE Transactions on Magnetics* **33**, 53–62 (1997). viii, 3, 4

[2] Serway, R. A. and Beichner, R. J. *Physics for Scientists and Engineers with Modern Physics Fifth Edition.* Saunders College Publishing, (2000). viii, 4

[3] Persad, C., Yeoh, A., Prabhu, G., White, G., and Eliezer, Z. *IEEE Transactions on Magnetics* **33**, 140–145 (1997). viii, 8

[4] Fair, H. D. *IEEE Transactions on Magnetics* **33**, 16–16 (1997). 1, 3

[5] Persad, C. *IEEE Transactions on Magnetics* **33**, 134–139 (1997). 5

[6] Barber, J. *The acceleration of macroparticles in a hypervelocity electromagnetic accelerator.* PhD thesis, Department of Engineering Physics, Australian National University, Canberra, Australia, (1972). 5

[7] Marshall, R. In *High Power-High Energy Pulse Production and Application.* Australian National University Press (1978). 5

[8] Engel, T., Neri, J., and Veracka, M. *IEEE Transactions on Magnetics* **44**, 1837–1844 (2008). 5

[9] Satapathy, S. and Vanicek, H. *IEEE Transactions on Magnetics* **43**, 402–407 (2007). 6

[10] Crawford, R. *IEEE Transactions on Magnetics* **31**, 138 (1995). 7

[11] Persad, C., Yeoh, A., Barton, A., and Marshall, R. Technical report, U.S. Army ARDEC Contractors, Austin, Texas, (1994). 8

[12] Matyac, M., Christopher, F., Jamison, K., Persad, C., and Marshall, R. *IEEE Transactions on Magnetics* **31**, 332 (1995). 8

[13] Holm, R. *Electric Contacts: Theory and Application.* Springer-Verlag, (1967). 8

[14] Rabinowics, E. *Friction and Wear of Materials.* J. Wiley & Sons, (1965). 8

[15] Kuhlman-Wilsdorf, D. Technical report, 1st EM Gun Armature Workshop, Eglin AFB, (1986). 8

[16] Parks, P. *Journal of Applied Physics* **67**, 3511 (1990). 9

[17] Barber, J. and Dreizin, Y. *IEEE Transactions on Magnetics* **31**, 96 (1995). 9

[18] Heyse, M. and Jamison, K. Technical report, USAF Wright Labs, Eglin AFB, (1994). 9

[19] Angeli, M., Cardelli, E., and Azzerboni, B. *IEEE Transactions on Magnetics* **33**, 37–42 (1997). 9

[20] Hildenbrand, D. J., Rapka, J. R., and Long, B. J. *IEEE Transactions on Magnetics* **33**, 74–79 (1997). 9

[21] Ferrentino, G. L. and Kolkert, W. J. *IEEE Transactions on Magnetics* **22**, 1470–1474 (1986). 9

[22] Knoth, E. A. and Challita, A. *IEEE Transactions on Magnetics* **33**, 115–118 (1997). 9

[23] Campbell, J. D. and Ferguson, W. G. *Phil. Mag.* **21**, 63 (1970). 10

[24] Zerilli, F. J. and Armstrong, R. W. *Journal of Applied Physics* **61**, 1816 (1987). 10

[25] Steinberg, D. J., Cochran, S. G., and Guinan, M. W. *Journal of Applied Physics* **51**, 1498 (1980). 10

[26] Johnson, G. and Cook, W. 541–547, (1983). 10, 21

[27] Brünig, M. and Driemeier, L. *International Journal of Plasticity* **23**, 1979–2003 (2007). 11

[28] Eakins, D. and Thadhani, N. *Journal of Applied Physics* **100**(7) (2006). 27